Trends in Analytical Chemistry 135 (2021) 116148

Contents lists available at ScienceDirect

Trends in Analytical Chemistry

journal homepage: www.elsevier.com/locate/trac

Microneedle based electrochemical (Bio)Sensing: Towards decentralized and continuous health status monitoring

Juan José García-Guzmán [1], Clara Pérez-Ràfols [1], Maria Cuartero**, Gaston A. Crespo*

Department of Chemistry, School of Engineering Science in Chemistry, Biotechnology and Health, KTH Royal Institute of Technology, Teknikringen 30, SE-100 44, Stockholm, Sweden

ARTICLE INFO

Article history:
Available online 10 December 2020

Keywords:
Wearable sensors
Microneedle (bio)sensing
On-body continuous monitoring
Transdermal interstitial fluid analysis
Health care monitoring

ABSTRACT

Microneedle (MN) based electrochemical (bio)sensing has become a growing field within the discipline of analytical chemistry as a result of its unique capacity for continuous, decentralized health status monitoring. There are two significant advantages to this exclusive feature: i) the ability to directly analyze interstitial fluid (ISF), a body fluid with a similar enough composition to plasma (and blood) to be considered a plentiful source of information related to biologically relevant molecules and biomarkers; and ii) the capacity to overcome some of the major limitations of blood analysis including painful extraction, high interferant concentrations, and incompatibility with diagnosis of infants (and especially newborns). Recent publications have demonstrated important advancements in electrochemical MN sensor technology, among which are included new MN fabrication methods and various modification strategies, providing different architectures and allowing for the integration of electronics. This versatility highlights the undeniable need for interdisciplinary efforts towards tangible progress in the field. In a context evidently dominated by glucose sensing, which is slowly being expanded towards other analytes, the following crucial questions arise: to what extent are electrochemical MN (bio)sensors a reliable analytical tool for continuous ISF monitoring? Which is the best calibration protocol to be followed for *in vivo* assays? Which strategies can be employed to protect the sensing element during skin penetration? Is there an appropriate validation methodology to assess the accuracy of electrochemical MN (bio)sensors? How significant is the distinction between successful achievements in the laboratory and the real commercial feasibility of products? This paper aims to reflect on those previous questions while reviewing the progress of electrochemical MN (bio)sensors in the last decade with a focus on the analytical aspects. Overall, we describe the current state of electrochemical MN (bio)sensors, the benefits and challenges associated to ISF monitoring, as well as key features (and bottlenecks) regarding its implementation for *in vivo* assays.

1. Introduction

Two principal driving forces have, over the past few years, given rise to a new analytical philosophy of decentralized clinical diagnosis. These are, more specifically, shortcomings which have been identified in the healthcare system and an ever-growing population, resulting in saturation of services as well as increasing costs. In this context, a multitude of research papers have been recently published on new paths for point-of-care (POC) diagnostic devices with the promise to gather valuable patient health information, from within their own homes [1–5]. Common among all these devices, is the objective of developing robust and reliable tools to detect biomarkers in assessing human health at any time and place. For this purpose, wearable sensor technology is the approach that seems to best fulfil all the requirements for implementation in POC protocols; the minimally invasive nature of this technology coupled with the possibility to perform the analysis without need of a medical expert are highly appealing features [6,7]. In particular, electrochemical (bio)sensors stand out among readout options because of their excellent analytical features (i.e., high sensitivity, fast response time, and versatility) and inherent characteristics (i.e., ease of miniaturization, simplicity, low cost) [8]. Furthermore, the implementation of different electroanalytical techniques (e.g.

* Corresponding author.
** Corresponding author.
E-mail addresses: mariacb@kth.se (M. Cuartero), gacp@kth.se (G.A. Crespo).
[1] Juan Jose Garcia Guzman and Clara Perez Rafols share the first author.

https://doi.org/10.1016/j.trac.2020.116148

List of abbreviation

8-HQS	8-hydroxyquinoline-5-sulfonic acid
AOx	alcohol oxidase
BISF	brain interstitial fluid
BSA	bovine serum albumin
CE	counter electrode
ChOx	cholesterol oxidase
CMRF	curable magnetorheological fluid
CNT	carbon nanotubes
COC	cyclic olefin copolymer
CSF	cerebrospinal fluid
CV	cyclic voltammetry
ECF	extracellular fluid
FcCOOH	ferrocene monocarboxylic acid
FGPC	functionalized graphene composite
f-MWCNT	functionalized multiwalled carbon nanotubes
GA	glutaraldehyde
GDH	glucose dehydrogenase
GluOx	glutamate oxidase
GOx	glucose oxidase
HPLC-MS	high-performance liquid chromatography coupled with mass spectrometry
ICU	intensive care unit
IrOx	iridium oxide
ISF	interstitial fluid
ISO	International Organization for Standardization
LOD	limit of detection
LOx	lactate oxidase
LRR	linear range of response
LSV	linear sweep voltammetry
MN	microneedle
MPA	3-mercaptopropionic acid
MPOx	methyl paraoxon
MTT	meal tolerance test
NP	nanoparticle
NW	nanowire
N-UNCD	nitrogen-incorporated ultrananocrystalline diamond
OGTT	oral glucose tolerance test
OPH	organophosphorus hydrolase
PANI	polyaniline
PB	phosphate buffer
PBS	phosphate-buffered saline
PCL	polycarprolactone
PEDOT	poly(3,4-ethylenedioxythiophene)
PEG	polyethylene glycol
PEGDA	poly(ethylene glycol) diacrylate
PEGDE	poly (ethylene glycol) diglycidyl ether
PEI	polyethyleneimine
PET	polyethylene terephthalate
POC	point of care
PPy/8-HQS	8-hydroxyquinoline-5-sulfonic acid
PVB	polyvinyl butyral
PVP	polyvynyilpirrolidone
RE	reference electrode
rGO	reduced graphene oxide
SC	stratum corneum
SST	stainless steel
TCA	terthiophene carboxylic acid
TMA	thiomalic acid
TMPTA	trimethylolpropane ethoxylate triacrylate
TRL	technological readiness level
UOx	uricase
U.S. FDA	United States Federal Food and Drug Administration
UV	ultraviolet radiation
VEGF	vascular endothelial growth factor
WE	working electrode

potentiometry, chronoamperometry, electrochemical impedance spectroscopy) and sensor development principles (e.g. ion-selective membranes, biofunctionalization) allow for the determination of a wide range of clinically relevant analytes, of both inorganic and organic nature [9,10].

The determination of health-related targets can be performed in different body fluids; at the time of writing blood and urine are the most heavily analyzed samples. However the spread of wearable sensors highlights the importance of analyzing easily body fluids beyond blood and urine, for instance sweat [11,12], tears [13] and saliva [14]. Note that the composition of these matrices is quite different from blood [15], and therefore, it not always the same kind of information which is obtained. Thus, correlation studies are of a paramount importance (despite being almost absent in the literature) to shed light on the utility of these sorts of analyses. In contrast, the interstitial fluid (ISF) seems to more precisely mirror the composition of blood serum [10]. Indeed, ISF is the fluid where body cells are embedded and has proven to be a rich source of biochemical information [6]. For example, Samavat et al. monitored glucose in ISF for 3 h and found acceptable correlation to concentration values observed through blood obtained by a finger-prick method [16]. Although ISF offers such advantageous opportunities, access to this fluid is limited by the physical barrier of the skin. Fortunately, microneedles (MNs) can overcome this barrier in order to reach ISF in a painless and effective manner. MNs are similar to intradermal needles but with microscale dimensions (typical length of 1000 μm) and have been widely investigated as a drug delivery platform, which currently represents a strong research field [17–21]. By contrast, employment of MNs in wearable electrochemical sensors is relatively recent. Results thus indicate a minimally invasive method involving painless skin insertion, which provides easy on-body portability and the possibility of implementation for the continuous biomarker monitoring.

The application of MN sensors would therefore be of primary benefit to the field of healthcare, as illustrated in Fig. 1. Facile and continuous monitoring of biomarkers is crucial in hospital facilities - in particular, Intensive Care Units (ICUs) – for patients ranging from adults to newborns; MN-based platforms could provide unprecedented real-time information about the patient's status and enable early medical actions, which would undoubtedly help to improve patient survival rates [22]. To demonstrate this significance, we have collected in Table 1 key analytes traditionally evaluated in ICUs, alongside their detection relevance and main diseases with which they are associated. It is not overly ambitious to believe that the great majority of these targets could be monitored in the future by MN sensors to assess a complete evaluation of patients' evolution, even as they experience a life-threatening condition such as sepsis. Besides ICU application, the use of MN sensors in emergency rooms, and for the daily monitoring of chronic patient status (in the clinic or even from their own home) would grant a measure of independence to end users. This would hence improve the life quality of lay citizens while decreasing the pressure on the health care system in terms of personnel, space and resources (economic gains). Another field in which MN sensors may

Fig. 1. Graphical concept. Application of microneedle-based sensors in the healthcare sector.

Table 1
Clinical relevance claimed for several analytes mainly considering reports on ICU environments.

Analyte	Priority	Related diseases	Ref
Sodium	Medium-High	Fluid loss, cystic fibrosis	[46–49]
Potassium	Medium	Arrhythmia, renal failure, sepsis, reduced gut motility, cystic fibrosis, spreading depression	[46–48,50]
Chloride	High	Sodium and acid-base disturbances, cystic fibrosis, spreading depression	[46–50]
pH	High	Metabolic and respiratory acidosis, sepsis, spreading depression	[50,51]
Calcium	High	Coagulopathy, osteopenia, neuromuscular excitability, cardiovascular complications, secondary hyperparathyroidism, myeloma	[52–54]
Phosphate	Medium	Osteopenia, arrhythmias, ventilatory insufficiency	[47]
Bicarbonate	Medium	Metabolic acidosis, renal-tubular dysfunction, sepsis	[51,55]
O_2 (PaO_2)	High	Lung failure, hypoxia	[56]
CO_2 ($PaCO_2$)	High	Lung failure, hypoxia	[56]
Glucose	High	Diabetes, occasions for hyper/hypoglucemia	[57]
Lactate	High	Sepsis, tissue hypoxia, arthritis, renal and hepatic diseases	[58,59]
Pyruvate	Medium	Renal and hepatic diseases, lactic acidosis	[58]
Uric acid	Medium	Gout, sepsis, kidney diseases	[60,61]
Creatinine	High	Sepsis, asphyxia, renal diseases (especially after renal replacement therapy)	[62]
Cortisol	High	Sepsis, stress	[63]
Adrenaline	High	Cardiac arrest, resuscitation	[64]
Bilirubin	High	Sepsis, acute respiratory distress syndrome	[65,66]

represent a remarkable potential for exploitation is that of health in sport. Continuous monitoring of several species – such as lactate or common ions (electrolytes) – while practicing physical activity would provide useful datasets that coaches and athlete support teams may use to optimize effort invested towards maximum reward at minimum health risk.

Despite this huge potential, efforts in the field thus far have been quite timid when compared with the forecasted capabilities of MN (bio)sensors. For example, recent efforts have been primarily devoted to glucose monitoring for diabetes control, with a great variety of research papers applying different methodologies [23–32]. Other metabolites such as lactate [33], alcohol [34], pH [35], cholesterol [36] or benzoquinone [37] have recently begun to attract more attention. Beyond reporting fabrication approaches and the required protocol for the analytical readout, only a small percentage of these papers has shown successful *in vivo* applications. In our opinion, one of the reasons for this lack of applications in real contexts is the necessity for non-toxic, biocompatible materials, and the need to assure that no substance can leak from the MN sensor into the body in question. Moreover, both the proper calibration and validation of MN (bio)sensors are still challenges that must be tackled in ISF transdermal analysis. One major obstacle to this process is the lack of suitable methods for extraction of ISF for validation purposes. Some approaches have been put forward [38], but as yet no clear methodology is available in the literature. Finally, both robustness and flexibility are mandatory properties for wearable sensors, even more strictly so in the case of sporting health applications due to the extreme movement range of the subjects. Taken altogether, this results in a disproportionately small market for commercial MN sensors which is dominated by a few examples of glucose monitoring devices [39,40].

Hence, the present review focuses on the main advances achieved in the electrochemical MN (bio)sensors field in the last decade. Other works have already thoroughly reviewed MN sensors

[41–45], but this is the first time that a review focuses entirely on the analytical viewpoint of electrochemical MN (bio)sensors. It should be stressed that our primary aim is to provide an accurate overview of this field, and that it is not our intention to disregard every work reporting on the electrochemical MN field during the selected period. All the data hereby presented were collected from the original research papers with the unique purpose to offer an exhaustive insight into the topic and analyze its current state. The first part of this review is dedicated to understanding the skin composition and the physical characteristics required for MNs to be able to painlessly reach ISF. Next, the *in vitro* analytical performance of the reported sensors is critically reviewed, highlighting the most successful approaches and deriving therefrom the most crucial parameters for success. Finally, a discussion regarding the main advances and difficulties encountered in the implementation of electrochemical MN sensors for *in vivo* analysis is provided, thereby envisioning the real market demands. Overall, this review seeks to provide a realistic insight on the most urgent aspects of the field, and the direction in which should future studies be focused.

2. Understanding the biology behind MN sensors

2.1. The skin: a complex organ in the human body

The MN has a double purpose in the wearable settings: (i) to disrupt the skin barrier to gain access to the ISF and/or blood, and (ii) to act as the platform for the sensing element. Evidently, to develop reliable and suitable MN sensors, it is crucial to first understand the skin structure. When measured by surface area, the skin is one of the largest organs in the human body (second only to the small intestine) with an average surface area in adults of around two square meters. Skin thickness presents a wide variability depending on the part of the body that is examined. For example, the thickest skin is to be found in the palms of the hand and the soles of the feet, while the thinnest skin is located around the eyelids [67]. The functions of this organ include protection against chemical, radiation and biological threats (bacteria, allergens and fungus), retainment of water and nutrients, heat regulation, water resistance, and adsorption/excretion processes. This versatile functionality of skin is related to its complex structure [68]. Due to this complexity, this review analyzes basic aspects on the structure, exclusively dealing with the aspects which have a direct guiding hand in the mechanical design of MN (bio)sensors for successful penetration. Briefly, the structure of skin can be understood as being composed of three layers: epidermis (outer layer), dermis (middle layer), and hypodermis (inner layer), as illustrated in Fig. 2 [69].

The epidermis thickness generally varies between 50 and 150 μm (thicker skin is found in palms and soles), and its cell composition ranges from anuclear cells in the outermost parts to hexagonal-shaped cells in the innermost. Epidermis is principally divided in two sublayers, *stratum corneum* (SC) and viable epidermis, with the first layer being lipophilic and the second hydrophilic. The SC is the external layer of epidermis, and it has been demonstrated that this layer constitutes the principal barrier towards drug penetration. SC thickness is about 10 μm but can reach 400 and 600 μm in the palms and soles. The viable dermis then, also known as the *stratum basale*, contains a higher water content than the SC [70], and demarcates the boundary line between the end of the epidermis and the beginning of the dermis. The thickness of the dermis varies between approximately 500 and 2000 μm and is composed primarily of fibroblasts, collagens and elastic fibers. Dermis is the skin layer where nerves, blood vessels, sweat glands and derma lymph nodes start to appear [41]. The pressure needed to penetrate this layer is about 1–5 MPa [71]. Finally, the innermost layer (hypodermis) is the thickest of all the three. Constructed out of connective tissues and fibrous collagen, in some regions of the body this wall can be several millimetres thick. Adipocytes, fibroblasts and macrophages occur in this area. In addition, nerves, arteries, veins and lymphatic glands are much more densely congregated in this zone. The hypodermis is relevant in several physiological pathways such as homeostasis, lipid regulation/fluid distribution, thermal equilibrium; moreover it acts as energy reservoir as well as providing bonding tissues to muscles and bones [70].

2.2. Interstitial fluid as an alternative source for obtaining chemical information

In the pipeline design of MN (bio)sensors, the very first thing to be selected is the biological fluid under study, this will define most of the mechanical properties required for the MN substrate (length, shape, rigidness, and thickness among others). In principal, as blood is considered the primary biological fluid source of biochemical information it is generally the first choice among such fluids for analysis. In addition, the composition of blood updates itself continuously as the health status of the patient changes. Blood vessels can be found in the dermis layer, to a depth ranging from 500 to 2000 μm depending on the body zone. According to the final dimensions needed for skin penetration, both macroscale needle and microneedle (MN) based sensors can be appropriate. However, we have found that all blood sensors in the literature tend to be referred to as MN blood sensors regardless of the actual dimensions, especially in terms of length [16,72]. The same applies to some cases involving MN sensors for cerebrospinal fluid (CSF) and organ tissue penetration during surgeries [73]. This is the result of unclear consensus in the general definition of a MN: in terms of length, the upper limit varies from 1000 to 2500 μm, while ranges of 50–250 μm and 1–25 μm appear to have been established for the base and tip diameter respectively [74–78]. In addition to this, blood analysis by means of MN sensors (in the most general context of dimensions) presents some drawbacks that should be stressed at this point: i) the large amount of interfering species present in blood can lead to severe fouling problems for sensors; and ii) an ideal continuous monitoring scenario with MNs should involve the least disruption possible for the patient, avoiding any interferences with normal activities and daily routines. Regarding this latter point, it is evident that the place for implanting the MN (bio)sensor should exceed traditional finger pricks measurements.

The use of ISF as an analytical fluid sample has the potential to overcome these limitations: ISF is found in the subcutaneous tissue and therefore can be accessed by MNs with reduced length and more painless insertion. This would in principal allow for a more accessible continuous monitoring over a period of hours to days, or even longer in an ideal case. Furthermore, MNs may provide a method of ISF collection for the purposes of validation [79]. Reverse iontophoresis is a further method that could potentially be put to this use [6]. For example, reverse iontophoresis was successfully applied for glucose detection using biosensors embedded into epidermal patches or devices (such as the GlucoWatch) with promising results [10,11]. However, special attention should be paid to the applied electrical pulses to avoid additional disturbance in the form of pain or even side effects to the patient. Indeed, this eventually proved a reason for the withdrawal of the GlucoWatch from the market [6].

In terms of composition, ISF is furnished with nutrients and oxygen by diffusion processes from the dermis, which is in turn refreshed by blood capillaries. This diffusion process is quite complex due to the involvement of both superficial plexus (300–600 μm in depth, contains small blood vessels) and lower

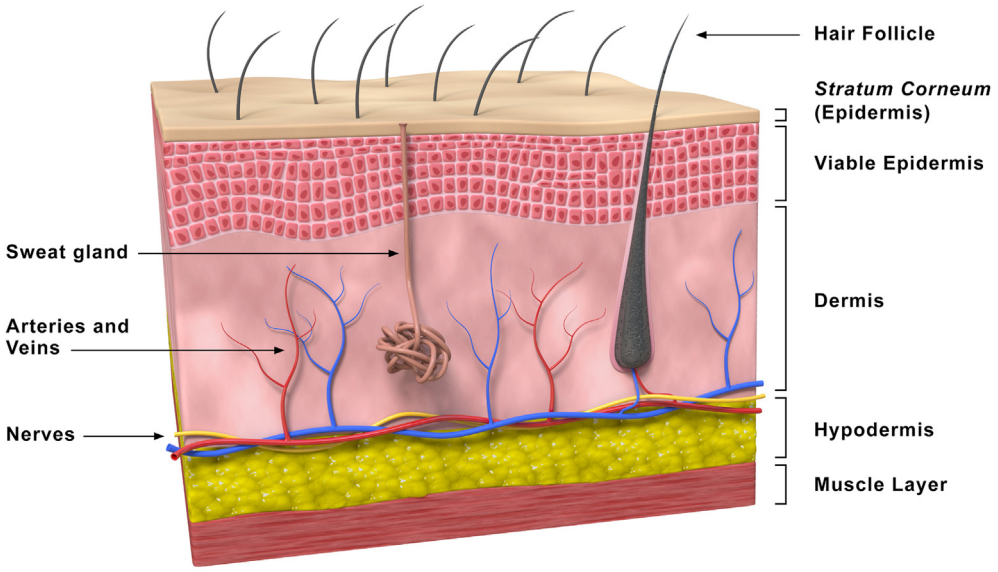

Fig. 2. Scheme of skin layers structure.

plexus (1300–1500 μm in depth, sustained by larger arteries and veins derived from muscles, lipids and subcutaneous tissues). As a result, there is a noticeable nutrient gradient along the skin, with a higher ratio of replenishment in the deeper zones [41]. Nevertheless, there is an equilibrium between ISF and plasma maintained by several small molecules (e.g. albumin, CO_2, phosphates) [80]. Thus, the composition of ISF is to some extent similar to blood with the exception of the absence of blood cells. Note that remarkable similarities in the protein (93.3%) [81], metabolites (79.3%) [82] and RNA (92.5%) [79] composition have been widely demonstrated. Slight differences include both a lower protein concentration and lower levels of some ions such as calcium, magnesium, sodium and potassium. Table 2 depicts normal values of the major metabolites and ions found in ISF and in blood for comparison. In the case of larger molecules such as glucose, a correspondence between both fluids can be observed. Nonetheless, fast changes in blood glucose are slowly encompassed (and therefore manifested) in ISF, with the rate being principally limited by the diffusion of these molecules through the endothelium [41]. Regarding this lag time, it has been demonstrated that there is an average time requirement of between 8 and 10 min to equilibrate concentrations in the two fluids, but even higher values (even 45 min) have been reported in some cases [69,83,84].

Overall, ISF shares enough composition with plasma (or blood) to be a valuable source of information regarding many biologically relevant molecules and biomarkers while avoiding the need for direct blood analysis. As an additional benefit, the issues of surface fouling are significantly decreased for ISF in comparison with blood as a result of the lower concentrations of proteins and other large molecules in this former [6], hence facilitating a long-term electrochemical readout. Thus, ISF analysis by means of MN (bio)sensors clearly represents a great potential towards the achievement of continuous monitoring in a minimally invasive assembly.

2.3. Requirements in MN geometrical and mechanical properties

Fig. 3 illustrates the main parameters to be considered in the development of MN sensors considering three key aspects: resistance to skin penetration, pain inflicted to the end-user, and target body fluid. In terms of resistance to skin penetration, parameters such as length, material type, shape, tip angle, and insertion force are important for the development of a robust device able to reach the SC (or even deeper) with minimal penetration effort and, as a result, minimal discomfort for the individual. To establish a suitable design, it is necessary to assess separately the distinct layers of SC, viable epidermis, and dermis. Each one displays different mechanical properties and depths, which can be affected by various factors such as body region, hydration level and even alimentary diet. Furthermore, skin viscoelasticity is another factor to deal with during penetration in *in vivo* assays [41].

Several studies have determined Young's Modulus for SC, viable epidermis and dermis, with the derived results being 1–1000 Mpa [92], 2–20 MPa [93] and 10 kPa [94], respectively. In addition, it has also been proved that the nonlinear viscoelasticity of skin is better addressed by high velocity procedures (1–10 m s^{-1}) [95] which allow a more reliable insertion. Regarding the required force, Davis et al. were pioneers in establishing a safety margin for several MN geometries based on the ratio between the insertion and the force required to collapse a MN [96]. Likewise, other authors have focused their research towards a better understanding of the insertion step and the influence of different mechanical properties of the needles, such as relationship between the axial and transversal fractures and the Young's Modulus of the material used [97], suitability of the base diameter for the insertion [98] and shape of the MN [99], among others.

Regarding the length of the MN, a compromise is needed between a few parameters: it must be long enough to penetrate the desired skin layer but not so long as to foment axial fracture. Overall, the ideal MN should have minimised tip radius (5–80 μm) to favor the insertion; sufficient base diameter (100–200 μm), wall thickness (5–60 μm) and Young's Modulus to avoid fractures; a well-designed tip geometry (i.e. conical, cylindrical, pyramidal) [99] to minimize the force required for the insertion; and appropriate length to reach the target body fluid (below 600 μm for ISF and *ca.* 1000–2000 μm for blood). Some viable dimensions and geometries that have been reported for MN electrochemical sensors targeting different biological fluids are summarized in Table 3, as possible reference for success. Nevertheless, the reader must notice that the majority of these papers are not demonstrated for *in vivo* applications despite claiming that the MN (bio)sensors have been designed for such purpose. On the other hand, while it seems indubitable that ISF can be reached by MN devices for sensing

Table 2
Normal values of the main metabolites and ions in blood and ISF.

Analyte	ISF concentration (mM)	Blood concentration (mM)	Ref
Total protein content	20.6 (g L^{-1})	73.7 (g L^{-1})	[85]
Albumin	0.188	0.676	[85]
Ca^{2+}	1.183	1.257	[85]
Mg^{2+}	0.506	0.532	[85]
Na^{+}	135.7	141.8	[85]
K^{+}	3.17	4.28	[85]
CO_2	23.9	29.7	[85]
Phosphate	0.610	1.117	[85]
pH	<7.35	7.35–7.45	[86]
Glucose	5.2 ± 0.8	4.9 ± 0.4	[87]
Lactate	1.12 ± 0.23	0.78 ± 0.18	[88]
Pyruvate	0.10 ± 0.01	0.12 ± 0.01	[88]
Glycerol	0.22 ± 0.03	0.038 ± 0.003	[88]
Urea	5.8 ± 0.4	4.8 ± 0.3	[88]
Total cholesterol	0.9 ± 0.2	4.4 ± 0.8	[89,90]
Glutamate	0.043 ± 0.008	0.042 ± 0.004	[91]
Alanine	0.25 ± 0.02	0.24 ± 0.03	[91]
Cysteine	0.034 ± 0.004	0.049 ± 0.002	[91]
Glycine	0.57 ± 0.09	0.194 ± 0.015	[91]
Serine	0.19 ± 0.02	0.10 ± 0.01	[91]
Total amino acids	2.61 ± 0.15	1.91 ± 0.08	[91]

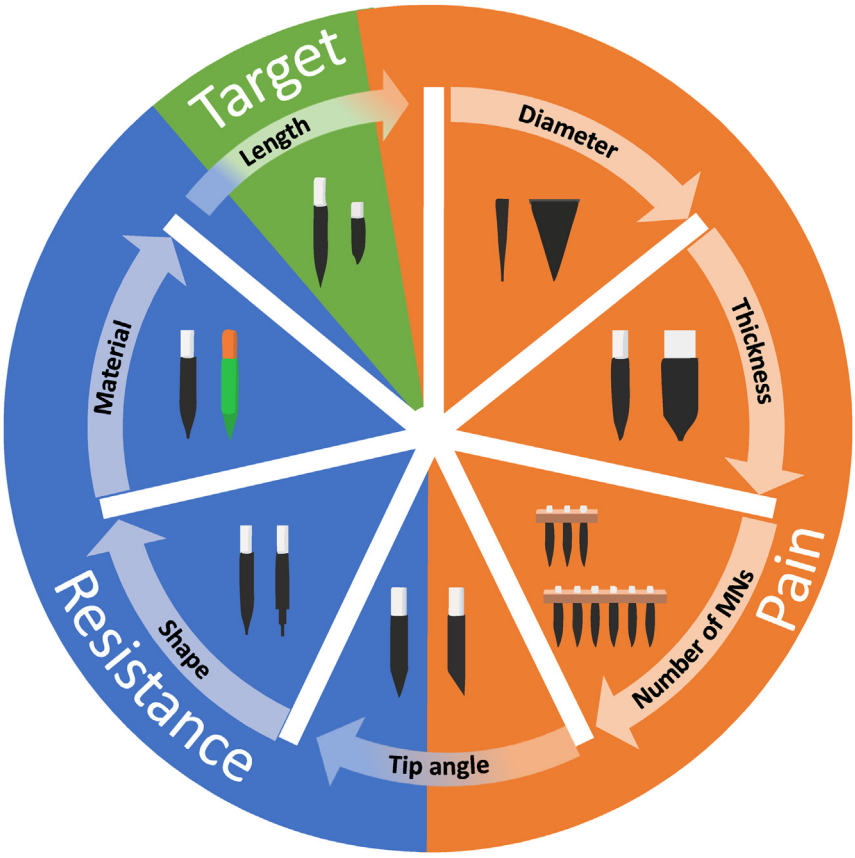

Fig. 3. Main features (target, pain and resistance) and their relationship with mechanical and geometrical parameters of the MNs.

purposes, their application in the analysis of blood, CSF or organ tissues could be questionable in terms of pain and invasiveness.

Discomfort or pain caused to the patient by insertion of the needles is an important aspect that must be considered. Accordingly, several studies have sought to quantify the pain caused by MNs and MN arrays to volunteers. Authors have evaluated the influence of several mechanical properties such as length, base diameter, thickness, number of MNs per array and tip angle [72,100,101]. Direct correlation between the pain caused to the patient and the length (up to 1450 μm) and number of MNs inserted (up to 50) was observed. Contrarily, no pain influence was noted in the assays with different thickness or tip angle, up to values of 100 μm and 90°, respectively. Finally, all patients stated that the pain imposed by MNs was always lower than that caused by the

Table 3
Physical characteristics and fabrication methods of MN sensors.

Type of MN	Substrate Material	Fabrication Method	Length (μm)	Base diameter (μm)	Tip diameter (μm)	Hole diameter (μm)	Biological fluid	Ref
Hollow	Polymer (Eshell 200) filled with carbon paste	Micromachining	700	800[a]	<10	–	ISF	[105]
Solid	Polymer (E-shell 200)	Computer assisted UV polymerization	818	390	NS	–	Serum[c]	[114]
Hollow	Polymer (E-shell 200)	Computer assisted UV polymerization	1366	1174[a]	NS	342	Serum[c]	[114]
Hollow	Proline/Silk/D-Sorbitol	Mold-filling followed by thermal curing	800	400	NS	NS	ISF	[23]
Solid	Polymer (PET)	Laser cutting	1500	700	NS	–	ISF	[134]
Solid	Poly(lactic acid)/*f*-MWCNT	Mold-filling followed by thermal curing	870	250	40	–	ISF	[122]
Hollow	Polymer (Eshell 200) filled with carbon paste	Computer assisted UV curing	1500	1250[a]	NS	425	ISF	[106–109]
Solid	Resin (TMPTA)	Mold-filling followed by UV curing	600	NS	200	–	ISF	[129]
Porous	Poly lactic-co-glycolic acid	Thermal drawing lithography followed by salt leaching	300	300	30	–	ISF	[27]
Hollow	Polymer (Eshell 200) filled with carbon paste	Computer assisted UV curing	800	NS	NS	425	ISF	[37]
Solid	Polycarbonate coated with Cr/Pt	Injection mold-filling	1000	600	40	–	ISF	[117]
Solid	Polycarbonate coated with Pt/IrOx	Injection mold-filling	1000	600	40	–	ISF	[118]
Hollow	Polymer (USP4)	Injection mold-filling	800	320–460	NS	100	ISF	[34]
Solid[f]	Polymer (PEG)	Mold-filling followed by UV curing	1000	300	NS	–	ISF	[135]
Solid	Polymer (PEGDA)	Photolithography	500	NS	NS	–	ISF	[131]
Hollow	Polymer (Eshell 300) filled with Au	Two-photon polymerization	1000	500	NS	NS	ISF	[110]
Solid	Polymer (SU8) coated with Ti/Pt	Mold-filling followed by UV curing	1000	600	35	–	ISF	[102]
Solid	Polymer (NOA68) coated with Au	Mold-filling followed by UV curing	280	190	<0.1	–	ISF	[31]
Solid	Polymer (SU8) coated with Au	Photolithography	200–400	73–136	38–101	–	ISF	[103]
Hollow	Polymer (E-shell 200) filled with carbon fibers	Computer assisted UV polymerization	1500	1200[a]	NS	400	ISF	[113]
Solid-	Polycarbonate coated with Au	Injection mold-filling	1000	600	20	–	ISF	[33,115,116]
Hollow	Polymer (Eshell 200) filled with carbon paste	Computer assisted UV polymerization	1500	1200[a]	NS	400	ISF	[112]
Solid	Polymer (COC) coated with Au	Mold-filling followed by thermal curing	700	100	NS	–	Blood	[24]
Solid	Polymer (SU8) coated with C	Mold-filling	1500	NS	NS	–	Blood	[16]
Solid	Polymer (SU8)	Photolithography followed by wet etching	3000	100 × 50[b]	NS	–	BISF	[104]
Solid	Polymer (PET) coated with Au/IrOx	Injection mold-filling	1600	800	50–80	–	Heart fluid	[136,137]
Solid	Carbon loaded polystyrene	Mold-filling followed by solvent evaporation	700	200	NS	–	Blood[d]	[130]
Solid	CMRF coated with Ti/Au	Magnetorheological drawing lithography	600	365	12	–	ISF	[120]
Solid	CMRF coated with Ti/Au	Magnetorheological drawing lithography	600	650	10	–	Serum[c,e]	[36]
Solid	CMRF coated with Ti/Au	Magnetorheological drawing lithography	700	185	5	–	NS	[121]
Solid	Stainless steel coated with Pt/rGO	Laser micromachining	800	225	NS	–	ISF	[124]
Solid	Stainless steel coated with carbon	Commercial	1000	450	15	–	ISF	[138]
Solid	Stainless steel	Laser microetching	680	250	200	–	ISF	[129]
Solid	Stainless steel coated with Pt	Commercial	680	250	NS	–	ISF	[139]
Solid	Stainless steel coated with AuNP/PtNP	Commercial	NS	180	NS	–	Blood	[140]
Solid	Stainless steel coated with Au and Pt black	Micromachining with a jet of ferric chloride	600	100	NS	–	Serum[c]	[26]
Solid	Stainless steel coated with C film/Ni_6MnO_8	Hydrothermal reaction calcination	1300	250	NS	–	NS	[125]
Solid	Tungsten coated with ZnO	Commercial	30,000	300	NS	–	CSF and bladder	[73]
Solid	Titanium coated with N-UNCD	Laser micromachining	340	230	10–20	–	ISF	[141]
Solid	Gold	Mold-filling followed by thermal curing	290	190	10	–	ISF	[128]
Hollow	Silicon	Photolithography followed by deep-reactive ion etching	150	100	<1	30	ISF	[127]
Hollow	Silicon	Deep-reactive ion etching followed by wet etching	400	NS	NS	30	ISF	[132]
Hollow	Silicon	Deep-reactive ion etching followed by anisotropic etching	700	260	–	90	ISF	[28]

(*continued on next page*)

Table 3 (*continued*)

Type of MN	Substrate Material	Fabrication Method	Length (μm)	Base diameter (μm)	Tip diameter (μm)	Hole diameter (μm)	Biological fluid	Ref
Solid	Si_3N_4 coated with Cr/Au	Photolithography followed by reactive ion etching	350	50	50	–	ISF	[126]
Solid	Silicon coated with Fe	Photolithography followed by deep-reactive ion etching	380	NS	<1	–	ISF	[32]
Hollow	Silicon	Laser micromachining	300–350	150	NS	50	ISF	[95,142]
Solid	Silicon coated with Au	Deep-reactive ion etching followed by wet etching	600	200	NS	–	Blood	[119]

BISF: brain interstitial fluid; CMRF: curable magnetorheological fluid; COC: cyclic olefin copolymer; CSF: cerebrospinal fluid; *f*-MWCNT: functionalized multiwalled carbon nanotubes; IrOx: iridium oxide; ISF: interstitial fluid; NP: nanoparticle; NS: not specified; N-UNCD: nitrogen-incorporated ultrananocrystalline diamond; PCL: polycarprolactone; PEDOT: poly(3,4-ethylenedioxythiophene); PEG: polyethylene glycol; PEGDA: poly(ethylene glycol) diacrylate; PET: polyethylene terephthalate; rGO: reduced graphene oxide; TMPTA: trimethylolpropane ethoxylate triacrylate; UV: ultraviolet radiation.

[a] Triangular.
[b] Non-circular.
[c] MNs were tested in serum aiming at further on-body blood detection.
[d] Horse.
[e] Bovine.
[f] Porous MN.

regular hypodermic needle insertion (outer diameter of 460 μm and insertion depth of 5 mm).

2.4. Materials and fabrication methods

The material(s) used and the type of MN are also key considerations in the design of MN (bio)sensors, to assure total compatibility with both the incorporation of the sensing element and its implementation for transdermal analysis. As observed in Table 3, the materials generally used to build MNs can be categorized into three main groups: polymers, metals and silicon. Most often, polymers are chosen due to their low cost and ease of manufacture. Thus, a great variety of polymers has been reported in the literature, including epoxy-based negative photoresists (e.g. SU8) [16,102–104], acrylate-based polymers (e.g. Eshell) [37,105–114] or polycarbonate [33,115–118], among others. It is common practice to modify the polymer fabrication in order to improve some specific features. For example, the electrical conductivity can be increased by coating polymeric MNs with metals, metal oxides or alloys such as Au [24,31,33,103,119], Pt/IrOx [118], Ti/Au [36,120,121] or Cr/Pt [117], Other approaches for conductive coatings are based on conductive forms of carbon such as carbon paste [37,105–109,112], carbon fibers [113] or carbon nanotubes [122]. Although less common, the coating of polymeric MNs can also have a more specific purpose. For example, Keum et al. modified polylactic acid MNs with the conducting polymer poly(3,4-ethylendioxitiophene) to establish a channel layer where the element of recognition for the analyte (hemin molecules for nitric oxide) could be placed [123].

In terms of metallic MNs, the most common substrates are Au, Pt, and W due to their excellent conductivity and biocompatibility. In addition, although less conductive, stainless steel is commonly found in the literature because of its high biocompatibility and lower cost. All of these metals can be further coated to improve conductivity (if necessary) but also with other goals, as discussed above for polymer-based MNs. For example, Jin et al. used Pt nanoparticles and reduced graphene to increase the electrocatalytic activity of stainless steel MNs towards the detection of hydrogen peroxide [124]. Jia et al. proposed the use of Ni_6MnO_8 nanoflakes to improve the surface adherence properties of stainless-steel MNs by providing a seed layer for further modifications with the ultimate aim being detection of ascorbic acid [125]. Importantly, MNs fabricated with potentially toxic metals (such as nickel or nickel alloys) can be coated with metals such as Au or Pd to improve their biocompatibility [30].

Silicon, in both its elemental state and as silicon nitride (Si_3N_4), is another material widely used in the fabrication of MNs due to its superior biocompatibility [126]. An interesting feature of hollow silicon MNs is that they also allow passive extraction of ISF through capillary actions [127]. Ribet et al. took advantage of this property in the development of a glucose biosensor, which was based on the integration of an ultra-miniaturized electrochemical sensing probe hosted in the bore of a hollow silicon MN (providing a physical protection during the insertion) and relied upon partial filling of the MN with ISF through capillary actions before reaching the probe [28].

Concerning the fabrication methods, MNs are generally obtained *via* one of four different paths depending on how the substrate is formed: mold-filling, lithography, micromachining and computer assisted polymerization. Mold-filling methods are very popular due to the versatility that they offer in terms of both MN shape and substrate nature. By means of this procedure, it is possible to design and fabricate a general mold with the desired geometry, and later proceed with the filling of the mold with the substrate material in liquid state. Despite the predominance of polymers, Senel et al. have demonstrated that metal-based MNs can also be produced in this manner using molds filled with metallic nanoparticles ink embedded in an organic solvent [128]. By convention the molding step is followed by a curing process that can be performed in different ways depending on the final substrate nature, where UV radiation [31,102,129], heat treatment [23,24,122,123] and solvent evaporation [130] are the most usual procedures.

Lithographic methods commonly use bulk materials to etch the desired shape and dimensions of the MN. The printing is primarily carried out *via* photochemical processes [103,131] or thermal drawing [27]. Magnetorheological drawing lithography [120,121] is also gradually gaining attention in this field. This method forms the shape of the MN by handling a magnetic field in a curable magnetorheological fluid, which is much simpler compared to traditional lithography and as an additional advantage does not require temperature control or light masking. The main drawback of this method, however, is the limited number of suitable magnetic fluids, which constitutes a considerable hindrance to versatility.

The third method for MN fabrication is based on micromachining, in fact the most commonly used procedure for metallic MNs (see Table 3). In this method, MNs are obtained from bulk material by way of highly refined, smooth cutting, with incisions usually but not exclusively made by laser [124,129]. This technique is however not restricted to metal based MNs; Chua

et al. demonstrated the use of laser micromachining for the fabrication of hollow silicon MNs [95], as an alternative to the traditional manufacturing process based on deep reactive ion etching, whereby the bulk Si substrate is brought into the desired shape by way of attack by ion containing plasma [28,132]. It is worthy of note that some authors have exploited both micromachining and lithography as complementary techniques in order to create improved MN: the main body of the MN is fabricated by lithography and micromachining is later employed for final detailing and sharpening [126,133].

The use of computer assisted polymerization has increased in recent years for MN fabrication. The most common approach involves the polymer E-Shell 200 [37,105–109,112,113] polymerized by UV radiation. Interestingly, E-Shell 200 is a common material compatible with 3D printing technology. This polymer provides structures with clinically desirable properties such as strength, water-resistance, and biocompatibility, and has therefore been traditionally employed in a wide variety of medical devices.

3. Electrochemical MN (bio)sensors: useful considerations for *in vitro* and *ex vivo* assays

Table 4 summarizes the most relevant electrochemical MN (bio) sensors reported over the last decade, according to the approach established for sensing the analyte. An especial focus has been placed on the following aspects: sensing element, modification strategy for introduction within the MN substrate, electroanalytical technique for readout, and analytical parameters presented. In addition, the calibration media, the target biological fluid and the analytical application (if any) are collected in Table 4, with a view to better evaluation of the possible projection/exploitation of each MN-based invention. In particular, such cases that have demonstrated *in vivo* applications are deeper analyzed in Section 4 (see below).

It is important to highlight that the majority of the figures of merit reported in the selected papers (Table 4) were obtained in a buffer medium; in general, experiments carried out in such a matrix overestimate analytical performances when compared to those carried out in artificial biological fluids [115,131]. More realistic features are observed in the latter, including biofouling, reduced sensitivities, and narrower linear ranges of response due to stronger matrix effects, all of which is indeed a closer analogy to real measurements in ISF or blood. Therefore, the reported analytical parameters for MN (bio)sensors should be carefully considered when seeking to interpret any results. In a typical report, the classical analytical parameters such as limit of detection (LOD), sensitivity, linear range of response (LRR), selectivity and reproducibility, in the selected medium of buffer or artificial fluid, are evaluated for MN sensors. However, considering the final *in vivo* application for continuous intradermal sensing, other aspects such as resistance to skin penetration or potential toxicological effects should also be assessed. Unfortunately, with a few exceptions which are elaborated upon below, we have found a distinct lack of such evaluation within the literature.

The procedures and materials utilized to fabricate the MN (bio) sensors have a strong influence in many transversal aspects related to the final analytical performance of the device and *in vivo* suitability. For example, one common strategy for the development of MN (bio)sensors consists of the external modification of solid MNs, thus facilitating a good interaction with the analyte [115,131]. But during skin penetration, the sensing element is entirely exposed to friction with the skin layers, or even to undesired substances present in the skin that can damage or alter the sensor features. One option to solve this drawback is the employment of an external water-soluble polymeric layer that protects the sensing element from mechanical alteration during skin penetration. Then, the layer is dissolved in ISF after penetration to allow for direct exposure to the target [124]. Another strategy used for the preparation of MN (bio)sensors is based on internal modification of hollow MNs, which provides a physical protection of the sensing element during the insertion and limits undesired contact with tissues, therefore reducing biofouling effect [23,112]. As observed in Table 4, 70.8% of the reported MN sensors are based on external modification and only 26.4% on internal modification.

Whatever the strategy used to incorporate the sensing element to the MN, it is evident that resistance to skin insertion should be always evaluated prior to any *in vivo* application to ensure that the analytical performance of the MN sensor is not affected by the insertion, nor once inside the skin. Studies of this type have been proposed through *in vitro* procedures by use of agarose hydrogel in contact with artificial ISF to mimic the real skin system [116]. This approach has been claimed in the literature to be useful in evaluating the resilience of the MN sensor by comparing the calibration graph before and after insertion in the gel. Such a set up was used to confirm that external calibration is suitable for the calculation of ISF concentrations through transdermal detection, by comparing the signals acquired through the agarose hydrogel at increasing analyte concentrations in artificial ISF with external measurements [105,116]. Another method considers the resilience of the external calibration after subsequent insertions into animal skin fixed in a physical support that allows for a contact with artificial ISF in which the analyte concentration can be manually changed, which is undoubtedly a closer approach to the real scenario than the use of gel [34,124,138].

Regarding cytotoxicity studies, it is important to ensure that no toxic effect is caused by direct contact, leaching, or detachment of the sensing element. Cytotoxicity assays evaluate cell viability after exposure to the sensor and/or its different components as compared to a control group of cells. The effects of direct contact between the sensor and the cells and of leaching/detachment of singular components, can be studied by means of different experimental configurations; that is to say, deposition of the sensor/components directly upon the wells for the former, and for the latter placement of sensor/components on top of the culture media (or by use of transwell scaffolds) [143]. Crespo and co-workers [138,143] performed a cytotoxicity assay with MN sensors for the determination of potassium based on ion-selective membranes. Human fibroblasts were used as cell line, and it was found that valinomycin (the potassium ionophore in the membrane) leached from the membrane and presented a severe toxic effect (cell viability of 17.9 ± 2.5%). Cell proliferation tests then demonstrated that the MN sensor was safe for continuous use over at least 24 h with no toxic effects. A similar study was reported by Tang et al. using human umbilical vein endothelial cells to assess the cytotoxicity of a MN sensor for the determination of nitric oxide [144]. Several sensor configurations were tested, and no toxic effect was observed in a 24 h timeframe, with the cell viability being higher than 90% in all cases. Due to the implanted nature of MN sensors, immune response should be assessed as well; however, this evaluation seems to be routine only for MNs designed for drug delivery [145]. The immune response studied in these scenarios usually refers more to the supplied pharmaceutical than the MN itself. In the case of MN sensors, the immune response is related to the biocompatibility of the device, which has been already reported in the literature [146]. Also, some timid efforts have been made in the direction of evaluating skin inflammation after sensor insertion [124,140,142,147].

We now consider as a whole the setup needed for the electrochemical readout. For a potentiometric or amperometric readout, it is required a two-electrode (working electrode, WE, and reference

Table 4
Summary of the preparation, analytical performances and applications of MN (bio)sensors reported in the literature in the last decade.

Type of MN	Sensing element	Modification strategy	Analytical technique	Analyte	Calibration media/Target biological fluid	Analytical parameters	Application	Ref
Solid	GOx	External: Electropolymerization in polydopamine using mussel protein as source	Amperometry	Glucose	NS/ISF	LRR: 0–22.2 mM	Beagle dogs, cynomolgus monkey and human volunteers (ISF)	[134]
Solid	GOx	External: Polymeric film (electropolymerization)	Amperometry	Glucose	PBS/ISF	LOD: 0.15 mM LRR: 0.15–30 mM	Human volunteers (ISF)	[102]
Solid	GOx	External: Enzyme mixed in pre-polymeric solutions	Amperometry	Glucose	PBS/ISF	LRR: 2–24 mM	None	[139]
Solid	GOx	External: Covalent bonding through MPA	CV	Glucose	PBS/ISF	LRR: 2.8–22.2 mM	None	[151]
Solid	GOx	External: Drop-casting in vessel (during MN formation)	Amperometry	Glucose	PBS/ISF	LOD: 1 μM LRR: 0–4 mM	None	[131]
Solid	GOx	External: Enzyme mixed in pre-polymeric solutions	Amperometry	Glucose	PBS with $MgCl_2$/ISF	LOD: 0.5 mM LRR: 0–10 mM	None	[152]
Solid	GOx	External: Covalent bonding through TMA	Amperometry	Glucose	PBS/ISF	LRR: 2–25 mM	Fluidic platform (PBS)	[103]
Hollow	GOx	Internal: Casting of silk-enzyme mixture on the cavity	Amperometry	Glucose	Artificial ISF/ISF	LRR: 1.7–10.4 μM	None	[23]
Hollow	GOx	Internal: Enzyme mixed with carbon paste	Power density	Glucose	Artificial ISF/ISF	LRR: 0–25 mM	None	[109]
Hollow	GOx	Internal: Mechanical dispensing of cross-linked enzyme	Amperometry	Glucose	PBS/ISF	LRR: 0–13.9 mM	Human volunteers (ISF)	[28]
Hollow	GOx	Internal: Enzyme mixed with carbon paste	Amperometry	Glucose	PBS/ISF	LRR: 2–12 mM	None	[112]
Solid	GOx	Non modified: enzymatic reaction takes place in solution	CV	Glucose	PBS with FcCOOH/ISF	LRR: 2–13.5 mM	None	[31]
Solid	GOx	External: Covalent bonding to TCA followed by electropolymerization	Amperometry	Glucose	PBS/Blood	LRR: 0.05–20 mM	Finger pricked human blood	[24]
Solid	GOx	External: Electrostatic entrapment	Amperometry	Glucose	PBS/Blood	LOD: 0.1 mM LRR: 0–20 mM	Anesthetized mice (blood)	[140]
Solid	GOx	External: Drop-casting	Amperometry	Glucose	PBS/Serum	LOD: 260 μM LRR: 2–12 mM	Spiked fetal bovine serum	[36]
Solid inside hollow[a]	GOx	Internal: Entrapment in polymeric film	Amperometry	Glucose	PBS/Serum	LOD: 0.1 mM LRR: 0.1–14 mM	None	[114]
Solid	GOx	External: Dispensing through nitrogen pulses	Amperometry	Glucose	PBS/BISF	LRR: 0–2.5 mM	Brain of anesthetized rats	[104]
Solid	GDH	External: Drop-casting	Amperometry	Glucose	Artificial ISF/ISF	LOD: 50 μM LRR: 0.1–10 mM	Artificial ISF through chitosan/agarose hydrogel	[115]
Solid-	GDH	External: Drop-casting	Amperometry	Glucose	Artificial ISF/ISF	LOD: 7 μM LRR: 0.5–5 mM	Artificial ISF through chitosan/agarose hydrogel	[116]
Solid	–	External: Electrodeposition of Pt black	Amperometry	Glucose	PBS/ISF	LRR: 3–20 mM	None	[32]
Solid	–	External: Electrodeposition of Pt black	Amperometry	Glucose	PBS/Serum	LOD: 23 μM LRR: 1–40 mM	Blood serum	[26]
Solid	LOx	External: Drop-casting	Amperometry	Lactate	Artificial ISF/ISF	LOD: 3 μM LRR: 10–100 μM	Artificial ISF through chitosan/agarose hydrogel	[116]
Solid	LOx	External: Drop-casting in vessel (during MN formation)	Amperometry	Lactate	PBS/ISF	LOD: 1 μM LRR: 0–1 mM	None	[131]
Solid	LOx	External: Enzyme mixed in pre-polymeric solutions	Amperometry	Lactate	PBS with $MgCl_2$/ISF	LOD: 0.5 mM LRR: 0–4 mM	None	[152]
Solid	LOx	External: Covalent bonding through TMA	Amperometry	Lactate	PBS/ISF	LRR: 2–25 mM	Fluidic platform (PBS)	[103]
Solid	LOx	External: Drop-casting	Amperometry	Lactate	PBS/ISF	LOD: 2.4 μM LRR: 10–200 μM	Spiked artificial ISF and spiked human blood	[33]
Hollow	LOx		Amperometry	Lactate	PBS/ISF	LRR: 2–12 mM	None	[112]

		Internal: Enzyme mixed with carbon paste						
Hollow	LOx	Internal: Enzyme mixed with carbon paste	Amperometry	Lactate	PBS/ISF	LOD: 0.42 mM LRR: 0.42–8 mM	None	[108]
Solid	LOx	External: Dispensing through nitrogen pulses	Amperometry	Lactate	PBS/BISF	LRR: 0–3 mM	Brain of anesthetized rats	[104]
Solid	UOx	External: Drop-casting	Amperometry	Uric acid	PBS/Serum	LOD:4 μM LRR: 0.1–1.2 mM	Spiked fetal bovine serum	[36]
Solid	ChOx	External: Drop-casting	Amperometry	Cholesterol	PBS/Serum	LOD: 440 μM LRR: 1–12 mM	Spiked fetal bovine serum	[36]
Solid inside hollow[a]	GluOx	Internal: Entrapment in polymeric film	Amperometry	Glutamate	Serum/Serum	LOD: 21 μM LRR: 21–140 μM	None	[114]
Solid	Urease	External: Polymeric membrane (Immersion with stirring)	Amperometry	Urea	Artificial ISF/ISF	LOD: 2.8 μM LRR: 50–2500 μM	None	[128]
Hollow	AOx	Internal: Polymeric membrane (drop-casting) on a wire	Amperometry	Alcohol	Artificial ISF/ISF	LRR: 5–80 mM	Artificial ISF through mice skin	[34]
Hollow	Tyrosinase	Internal: Enzyme mixed with carbon paste	Amperometry	Levodopa	Artificial ISF/ISF	LOD: 0.25 μM LRR: 20–300 μM	Artificial ISF through mice skin	[106]
Hollow	–	Internal: Non-modified carbon paste	SWV	Levodopa	Artificial ISF/ISF	LOD: 0.5 μM LRR: 5–100 μM	Artificial ISF through mice skin	[106]
Hollow	OPH	Internal: Enzyme mixed with carbon paste	SWV	MPOx	PB/ISF	LOD: 4 μM LRR: 20–180 μM	Mice skin soaked in PB	[107]
Hollow	OPH	Internal: Polymeric membrane (deposition on surface)	SWV	MPOx	Artificial ISF/ISF	LOD: 10 μM LRR:10–160 μM	Artificial ISF through agarose hydrogel	[105]
Hollow	–	Internal: Non-modified carbon paste	SWV	Fentanyl	Artificial ISF/ISF	LRR: 10–200 μM	None	[105]
Hollow	–	Internal: Non-modified carbon paste	SWV	Norfentanyl	Artificial ISF/ISF	LRR: 40–400 μM	None	[105]
Hollow	–	Internal: Non-modified carbon paste	SWV	Morphine	Artificial ISF/ISF	LRR: 20–140 μM	None	[105]
Solid	Pt/rGO	External: Dip coating followed by thermal reduction	Amperometry	H_2O_2	PBS/ISF	LRR: 0.1–0.6 mM	Pigskin tissues soaked in PBS and mice	[124]
Solid	ZnO NWs/Pt	External: Sputtering	Amperometry	H_2O_2	PBS/ISF	LRR: 0–9 mM	Anesthetized mice (ISF)	[129]
Hollow	–	Internal: Non-modified carbon paste	Amperometry	H_2O_2	PBS/ISF	LOD: 20 μM LRR: 20–500 μM	None	[108]
Hollow	Pd	Internal: Electrodeposition	CV	H_2O_2	PBS/ISF	LOD: 15 μM LRR: 100–500 μM	None	[113]
Solid	PANI/MoS_2/PtNP	External: Electropolymerization	Amperometry	H_2O_2	PBS/cells release	LOD: 0.686 μM LRR: 1–100 μM	Living HeLa cells release	[153]
Solid	Ni_6MnO_8	External: Hydrothermal reaction-calcination	Amperometry	Ascorbic acid	NaOH/Vitamin C tablets	LOD: 0.1 μM LRR: 1–2000 μM	Vitamin C tablets	[125]
Solid	–	External: directly molded with poly(lactic acid) and CNT composite	DPV	Ascorbic acid	PBS/ISF	LOD: 180 μM LRR: 0.2–1 mM	Porcine ear skin soaked in PBS	[122]
Solid	–	External: Electrochemical anodization	SWV	Uric acid	Britton Robinson buffer/Blood	LOD: 2.8 μM LRR: 50–300 μM	Spiked horse blood	[130]
Solid	N-UNCD	External: Microwave plasma chemical vapor deposition	LSV	Uric acid	PBS/ISF	LRR: 2–200 μM	None	[141]
Solid	N-UNCD	External: Microwave plasma chemical vapor deposition	LSV	Dopamine	PBS/ISF	LRR: 0–30 μM	None	[141]
Hollow	–	Internal: Filling with organogel	Stripping voltammetry	Propranolol	Physiological buffer/NS	LOD: 50 nM LRR: 50–200 nM	Artificial saliva	[133]
Hollow	Catechol	External: Agarose hydrogel (drop-casting)	Amperometry	Tyrosinase	Phantom gel/ Melanoma	LRR: 0–4.5 μM	Porcine skin loaded with tyrosine	[37]
Solid	PEI/CNT	External: Dip-coating	Amperometry	DNA	Tris buffer/NS	NS	None	[126]
Solid	FGPC	External: Electrodeposition	Amperometry	NO	PBS/Blood	LOD: 3.2 nM LRR: 5–200 nM	Anesthetized rats	[144]
Solid	Hemin	External: Immersion	Amperometry	NO	PBS/Polyps	LOD: 1 μM LRR: 0–16 μM	Mice with and without melanoma (ISF)	[123]

(*continued on next page*)

Table 4 (*continued*)

Type of MN	Sensing element	Modification strategy	Analytical technique	Analyte	Calibration media/Target biological fluid	Analytical parameters	Application	Ref
Solid	Gold	External: sputtering	Amperometry	O_2	KNO_3/Biofilm	LOD: 3.4 μM LRR: 0–0.25 μM	Heterotrophic biofilm cultivated in a flat-plate bioreactor	[154]
Hollow	–	Internal: Nafion membrane on a Pt wire	CV	O_2	PBS/ Intramuscular tissue	LOD: 4.57 μM LRR: 9–1239 μM	Vascular blood (*ex vivo*) and intramuscular tissue (*in vivo*)	[149]
Solid	Quinone groups	External: Electrochemical anodization	SWV	pH	Britton Robinson/ISF	NS	Tomato skin	[35]
Hollow	Fast Blue RR	Internal: Deposition on carbon paste	CV	pH	PBS/ISF	LRR: 5–8	None	[112]
Solid	PANI/MoS_2	External: Electropolymerization	Potentiometry	pH	PBS/CSF	LRR: 3–9	Rat brain, anesthetized	[155]
Solid	ZnO	External: Sputtering	Potentiometry	pH	Buffer (NS)/CSF and bladder	LRR: 2–9	CSF and bladder of anesthetized mice	[73]
Solid	IrOx	External: Electrodeposition	Potentiometry	pH	Buffer (NS)/ Heart	LRR: 4–8	Explanted rat hearts	[136,137]
Solid	Valinomycin	External: Polymeric membrane (drop-casting)	Potentiometry	Potassium	Artificial ISF/ISF	LOD: 12.6 μM LRR: 0.063–63 mM	Artificial ISF through animal skin	[138]
Hollow	Valinomycin	In chip: Polymeric membrane (drop-casting)	Potentiometry	Potassium	NS/ISF	LOD: 2.2 μM LRR: 0.01–10 mM	Fluidic chip (matrix NS)	[111]
Hollow	8-HQS	External: Polymeric membrane (electropolymerization)	Potentiometry	Cu (II)	pH 5 (NS)/NS	LOD: 10 μM LRR: 10–1000 μM	Spiked tap water and juices	[156]
Solid	β-lactamase	External: Polymeric membrane (drop-casting)	Potentiometry	Penicillin-G	Artificial ISF/ISF	LRR: 0–4.3 mM	None	[118]
Solid	β-lactamase	External: Hydrogel (drop-casting)	Potentiometry	Penicillin	PBS/ISF	LOD: 6.8 μM	Human volunteers	[148]
Solid	β-lactamase	External: Hydrogel (drop-casting)	Potentiometry	Phenoxymethylpenicillin	Human ECF/ Human ECF	LOD: 0.5 μM	Human volunteers	[157]
Solid-	β-lactamase	External: Polymeric membrane (drop-casting)	Potentiometry	Amoxicillin	Artificial ISF/ISF	LRR: 0–6.9 mM	None	[118]
Solid	β-lactamase	External: Polymeric membrane (drop-casting)	Potentiometry	Ceftriaxone	Artificial ISF/ISF	LRR: 0–110 μM	None	[118]
Solid	VEGF aptamer	External: Coating	Capacitance	VEGF protein	Blood serum/ Blood serum	LRR: 0.1–1000 pM	None	[119]
Solid	Biotinylated BSA	External: Molecular binding	Impedance	Streptavidin	PBS/NS	NS	Fluidic chip (PBS)	[158]

8-HQS: 8-hydroxyquinoline-5-sulfonic acid; AOx: alcohol oxidase; BISF: brain interstitial fluid; BSA: bovine serum albumin; ChOx: cholesterol oxidase; CNT: carbon nanotubes; CV: cyclic voltammetry; ECF: extracellular fluid; FcCOOH: ferrocene monocarboxylic acid; FGPC: functionalized graphene composite; GA: glutaraldehyde; GDH: glucose dehydrogenase; GluOx: glutamate oxidase; GOx: glucose oxidase; ISF: interstitial fluid; IrOx: iridium oxide; LOD: limit of detection; LOx: lactate oxidase; LRR: linear range; LSV: linear sweep voltammetry; MPA: 3-mercaptopropionic acid; MPOx: methyl paraoxon; NP: nanoparticles; NS: not specified; N-UNCD: nitrogen incorporated ultrananocrystalline diamond; NW: nanowire; OPH: organophosphorus hydrolase; PANI: polyaniline; PB: phosphate buffer; PBS: phosphate-buffered saline; PEI: polyethyleneimine rGO: reduced graphene oxide; TCA: terthiophene carboxylic acid; TMA: thiomalic acid; UOx: uricase; VEGF: vascular endothelial growth factor.

[a] Solid MN are placed inside hollow MN to facilitate the entrapment of the enzyme.

electrode, RE) or three-electrode setup (as before with the addition of a counter electrode, CE), whereby the WE comprises the sensing element. The appropriate technology for providing MN-based CE and RE elements of electrochemical readout has advanced in parallel with the development of WEs. Thus, it is possible to integrate all of the necessary electrodes into separate MNs [138], or all within one single MN; in the latter case internal modification is evidently necessary [28].

Upon scrutiny of the literature, it becomes apparent that there is a trend of utilizing approaches which are well established for classical electrode formats in preparing the CE and RE. Thus, the RE may consist of an Ag wire somehow fixed within the MN [23,106] acting as pseudoreference electrode by providing a potential that is stable enough to be used in many amperometric sensors. A more stable potential is provided by Ag/AgCl electrodes prepared as chlorinated silver wires embedded in hollow MNs, or by some external modification of the MN such as: i) coating the MN with Ag/AgCl ink [124,129]; ii) treatment of a silver-coated MN with sodium hypochlorite solution for 30 s [148]; iii) treatment of silver wire or silver-coated MNs with a saturated solution of $FeCl_3$ [118,133,147]; and iv) anodization of silver wire placed inside the MN in a saturated solution of 3 M KCl for 2 min [149], among others. For the latter, long-term stability was enhanced by coating the RE with a Nafion layer, which also provides enhanced biocompatibility and a non-interfering environment [149].

Although the preparation of these Ag/AgCl REs is simple and versatile, they are in general rather sensitive to the chloride ion concentration in the ISF (or any sample), meaning that any significant deviation between the chloride concentration with respect to the calibration solution will lead to an error in quantification of the analyte when a potentiometry readout is used [35], due to a change in the potential provided by the RE. An enhanced potential stability may be provided by coating the Ag/AgCl wire or MN with the so-called reference membrane containing polyvinyl butyral (PVB) as polymeric matrix with NaCl in saturation levels. An additional external polyurethane layer has also demonstrated prevention of chloride leaching from the reference membrane, thereby maintaining a constant potential independent of the chloride concentration in the sample [138,150]. Concerning the CE, the most common approaches employed in amperometric measurements are based on platinum wires inside the MN [34,105,149] or MNs coated with platinum [124,129].

The final integration of the WE, CE and/or RE can be accomplished either in only one or separate MNs. Fig. 4 shows some representative electrode configurations published in the literature. A first approach consists of two different MNs (one for the WE and the other for the RE) for the potentiometric determination of potassium (Fig. 4a) [138]. In this case, both MNs are solid stainless steel MNs externally modified *via* drop-casting and fixed in a polymeric base. A similar approach using three separate MNs (WE, RE and CE) (Fig. 4b) was employed by Mishra *et* al. for the amperometric detection of methyl paraoxon [107]: polymeric hollow MNs were packed with carbon paste (WE and CE) or internally modified with Ag/AgCl ink (RE). The carbon paste in the WE was further modified with organophosphorus hydrolase (enzyme). In contrast, Fig. 4c and d display some configurations illustrating insertion of all electrodes in one single needle, which is particularly advantageous in studies where the sensor implantation is considered but evidently more challenging in terms of fabrication efforts than providing separate MNs [104,149]. In particular, Fig. 4c displays the internal design of a MN for the simultaneous detection of glucose and lactate (with the corresponding enzyme patterner in a Pt lattice) together with a control electrode (same substrate but modified only with BSA to check non-specific currents), which was used for *in vivo* studies in rat brain [104]. One disadvantage here is that the analyzed fluid should entirely fill the MN in order to provide reliable measurements for the three analytes, as the CE and RE are placed on the top of the device. Then, in the system presented in Fig. 4d, all the electrodes reach the same depth, with the sensor chip and hand-made electrical connections placed on top of the base in where the MN containing the electrodes is fixed [28]. In all the cases, the mission of the MN base is to provide an epidermal patch in which the requisite MN(s) are fixed for an established penetration depth. Thus, assemblage of the MN(s) in the base can be performed either by fixing first the MN(s) and subsequently tailoring them with the sensing and electrochemical element(s) [34,107], or by affixing the MN(s) once they are prepared [28]. The materials most widely used for the MN base are Eshell [37,106] and PDMS [17,138]. In particular, bases combining the property of adequate skin adherence with total biocompatibility and flexibility are desired for optimal adaptation to the subject's movements.

A cursory inspection of Table 4 reveals that the analyte most widely analyzed with MN sensors is glucose, followed by lactate, pH, and hydrogen peroxide; alcohol, uric acid, and potassium. MN sensors seem to make more use of ISF than blood analyses, which is in principle expected according to the philosophy of avoiding blood tests. Next, we present a detailed discussion of MN (bio)sensors reported in the last decade collected in Table 4, attending to two main groups: enzymatic or non-enzymatic sensors. Additionally, a final section discusses sensor arrays for the simultaneous determination of various analytes.

3.1. Enzymatic sensors

3.1.1. Glucose detection

The need for a POC tool for the continuous monitoring of diabetes incidence in society has meant that continuous glucose monitoring became the first milestone in the sights of MN sensing technology development. Clinicians and researchers in the field are in general agreement on this importance and, accordingly, some elegant reviews exclusively dedicated to glucose monitoring with wearable devices and/or MN sensors have been already published [25,69,78]. Traditionally, glucose has been electrochemically determined by enzymatic sensors since 1962, when Clark et al. proposed a successful biosensor based on glucose oxidase (GOx) [159]. This path has been extensively explored, even with MN sensors, resulting in a considerable number of publications and the release of a few commercial devices, which will be discussed in the last section of this review. As observed in Table 4, different strategies for GOx immobilization on the MN substrate have been investigated with regards to amperometric glucose detection.

From an analytical point of view, one key parameter that should be assessed to guarantee continuous glucose monitoring within the expected physiological range is the LRR. This concept can indeed be extended to any other analyte. Measurements obtained through skin insertion are not compatible with any type of sample treatment or dilution, being purely on-body measurements from temporary sensors implanted through and/or over the skin, and therefore, the obtained LRR must cover both normal and abnormal glucose levels (without any pre-treatment consideration). Normal glucose levels in blood are usually between 3.3 mM and 5.5 mM during fasting periods and up to 7.8 mM within 2 h of eating. Blood glucose levels of 8.8 mM are considered high and in extreme cases values of 20 mM have been reported. In contrast, glucose levels in ISF are not as well-known as those in blood, although some studies have assured a correlation between values found in the two fluids when the subject's body is in equilibrium (i.e. no net tendency to change) [160,161]. However, rapid changes in body glucose levels do not manifest in ISF as fast as in blood, due to the glucose diffusion from plasma to ISF as defined in previous sections [28].

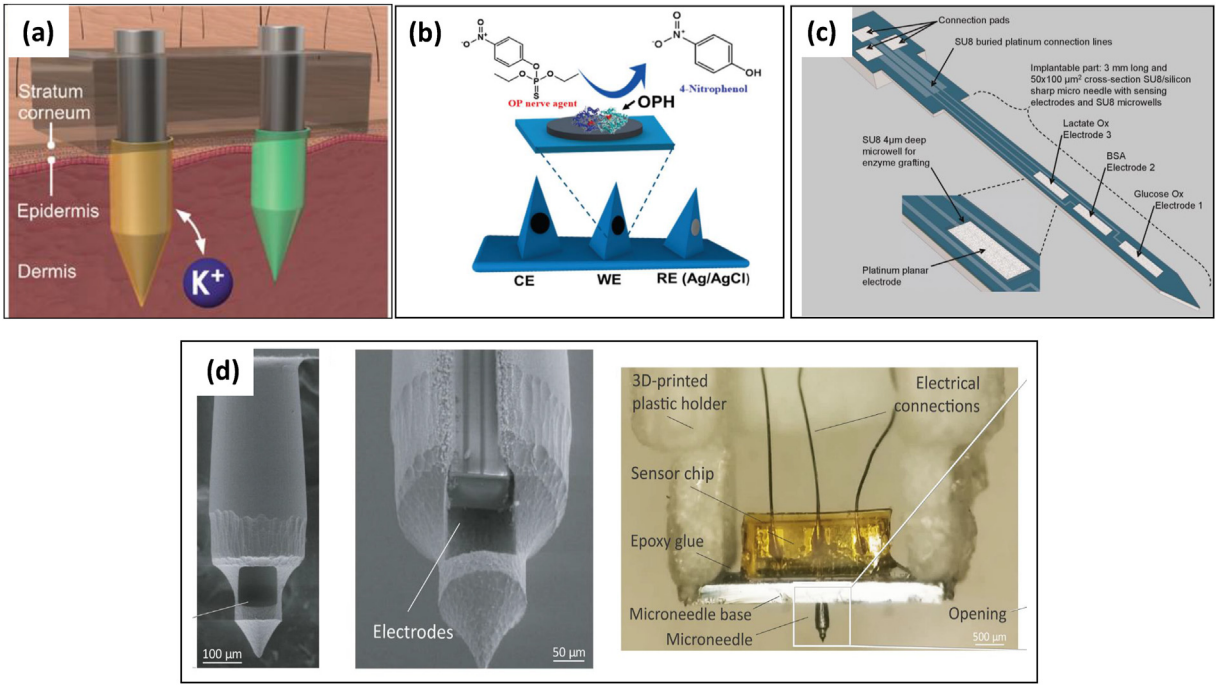

Fig. 4. Examples of modification strategies for MN sensors aiming for *in vivo* analysis. a) Two separate MN (WE and RE) externally modified for the potentiometric determination of potassium (Reproduced with permission from Ref. [138]), b) Three separate MN (WE, RE and CE) internally modified for the amperometric determination of methyl paraoxon (Reproduced with permission from Ref. [107]), c) Single MN containing 2 WEs and 1 control electrode distributed along its length for the simultaneous amperometric determination of glucose and lactate (Reproduced with permission from Ref. [104]), d) Single MN containing 3 electrodes (WE, RE and CE) for the amperometric determination of glucose (Reproduced with permission from Ref. [28]).

Assuming the same glucose concentration range in blood and ISF, adequate LRRs have been achieved with different MN sensors, with the majority of examples making use of external polymeric layers (such as Nafion or polyurethane) to provide appropriate analyte diffusion into the enzyme element, as well as to control the response of the biosensor towards certain interferants (such as ascorbic and uric acid) [16,103].

Other factors that should be considered are enzyme stability, overall lifetime of the sensor, and the effect of some physiological parameters prone to change during *in vivo* measurements (e.g., temperature, pH, conductivity, etc). Unfortunately, as far as we have been able to ascertain in the reported literature, these prospects are not rigorously evaluated at the *in vitro* stage despite being crucial to the achievement of *in vivo* applications and reliable clinical devices. Firstly, the developed MN biosensors should be stable for long periods of time under well-defined (and easy to achieve) storage conditions. While enzyme stability seems to be somehow improved or controlled with an appropriate immobilization method (i.e. adsorption in layer architectures [140], covalent bonding [24], cross-linking and physical entrapment [140,158], as can be seen in Table 4)[162], the optimization of storage conditions is also essential to maximize the lifetime of the MN biosensor preparation.

Regarding the effect of changes in the initial composition of the physiological fluid under study during *in vivo* (on-body) measurements, it is well-known that drastic changes in pH, temperature and sometimes conductivity affect the response of any enzyme, natural or engineered. Accordingly, the effect of these parameters in the biosensor response must be addressed, not only for GOx sensors, but for any other (bio)sensor exposed to the effects of these conditions. It would be convenient to measure at least pH and T also with MN based sensors, in order to provide an algorithm for the dynamic correction of the (bio)sensor response according to localised changes, in order to maximize the accuracy of the developed device. To the best of our knowledge, correction of this sort is lacking in the literature. As a guide for the reader, our research group has been recently working in this direction in the development of a wearable epidermal patch for glucose detection in sweat [12,163]. Similar strategies would undoubtedly benefit the MN sensor field towards trustworthy clinical POC solutions.

In general, traditional glucometers using human blood ("finger pricked") serve to evaluate the accuracy of the results provided by MNs reported for glucose analysis in ISF; evidently this validation only holds when assuming equal concentration of glucose in both fluids, taking into consideration the delay caused by diffusion from blood to ISF. Kim et al. developed a glucose MN biosensor by means of the following procedure [24]: a connector, insulator and spacer (with micro-holes) were joined prior to placing a MN mold on top and polymerizing the MNs. Subsequently a gold layer was electrodeposited covering all the MNs (WE, RE and CE), and the WE was externally modified by covalent bonding of GOx to a monomer (terthiophene) by a carbodiimide/N-hydroxysuccinimide reaction *via* CV onto the gold coated MN array. Finally, the whole sensor was coated with a Nafion layer. Amperometry in 0.1 M PBS (pH 7.4) was used for glucose calibration, achieving a LRR of 0.05–20 mM. An interesting feature of this work is the integration of a miniaturized portable potentiostat and a reusable wireless transmitter that can send the measured values to a mobile phone *via* Bluetooth. These elements were assembled in a transmitter with the MN array located in the lower part and placed on top of a measuring cell (Fig. 5). The incorporation of these two elements is fundamental in taking steps towards real market applications of continuous glucose monitoring. Although this paper presented a high level of integration, the performance of the entire device was tested only *ex vivo* with blood samples subjected to a dilution factor of 100. Although the LRR provided by the MN sensors was sufficient to cover blood glucose levels, this dilution was necessary to increase

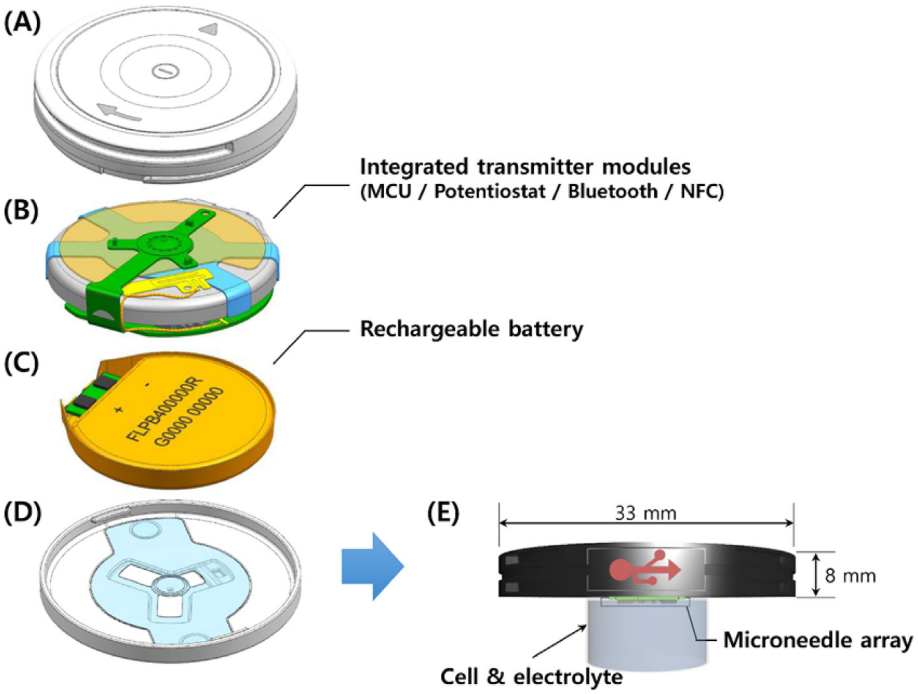

Fig. 5. Transmitter consisting of (A) top cover with an on/off button, (B) integrated transmitter modules, (C) lithium-ion polymer battery and (D) bottom cover with the microneedle. (E) Assembled transmitter with 33 mm diameter and 7.5 mm height coupled to the measuring cell. Reproduced with permission from Ref. [146]).

the volume of the sample in order to fill the measuring cell in which the MN biosensor was immersed. The obtained glucose concentration in the samples was compared with a commercial glucose monitoring equipment, showing good correspondence.

It is of note that GOx is not unique as an available enzyme for the development of glucose biosensors; glucose dehydrogenase (GDH) has also been reported for this purpose (see Table 4). Bollella et al. used GDH and 6-(ferrocenyl)hexanethiol (redox mediator) embedded within a gold MN array with the aim of enhanced sensor selectivity [115]. Indeed, selectivity studies showed that D-fructose, D-mannitol, D-galactose and ascorbic acid did not show a significant response (being lower than 10% of the signal registered for glucose at equivalent concentrations). In terms of stability, the sensor presented a rather stable signal for 30 days (with 80% of the initial signal being recorded after this period). The calibration was performed in artificial ISF and the LOD and LRR obtained were 50 μM and 0.1–10 mM respectively, which are acceptable for both healthy and diabetic samples. The influence of the temperature and pH on the biosensor response was also studied, achieving optimal results at pH 7 and 35°C. However, this kind of optimization is not very useful in the case of MN sensors because neither pH nor temperature can be adjusted during *in vivo* assays. However, these data could be used for further correction of the sensor response, as suggested in the previous section. Also, sensor performance was by insertion in chitosan/agarose hydrogel embedded with ISF as a skin-mimicking model. Two different glucose concentrations were tested simulating low and high glucose levels (4 and 8 mM), demonstrating that the insertion did not hinder the sensor performance.

3.1.2. Detection of other analytes

After glucose (according to Table 4) the molecule most frequently analyzed by MN biosensors is lactate. Blood lactate levels range from 0.60–0.96 mM in basal conditions [87] to 12–25 mM during physical exercise or in abnormal body situations such as cardiac diseases [164]. Importantly, most of the reported MN biosensors cannot reach the required LRR (*ca.* 0.5–25 mM, Table 4) for the reliable detection of lactate in blood and also in ISF, since similar levels are expected in both fluids. While the detection of basal conditions is generally quite facile, saturation problems hinder the determination of higher concentrations, with the upper limit of linearity reaching 8–12 mM in best-case scenarios (see Table 4) [108,112]. Note that this problematic is not a particularity of MN lactate biosensors, but instead constitutes a limitation for any amperometric detection of lactate with enzymatic sensor [165]. Further fundamental research is undeniably still needed in this direction for any subsequent application to MN technology.

Commonly, lactate sensors are based on lactate oxidase (LOx), which oxidises lactate with the release of hydrogen peroxide that is then detected through a redox mediator. This is the strategy followed by Bollella et al., who externally modified an array of gold MNs, immobilizing LOx (by drop-casting) on a nanocomposite surface (Au-multiwalled carbon nanotubes) that contained methylene blue as redox mediator [33]. The calibration was performed in amperometry mode in 50 mM PBS (pH 7.4), achieving a LOD of 2.4 μM and LRR of 10–200 μM, still very far from the required concentration range. Stability tests were conducted by carrying out 20 measurements of a 0.2 mM lactate solution daily, with storage of the electrode in the fridge when not in use. The sensor presented *ca.*10% loss of the initial response after 30 days. No appreciable interference was observed in the presence of ascorbic acid, uric acid, or glucose. The analytical performance of the sensor was tested in artificial ISF and human serum samples, obtaining an even narrower LRR and lower sensitivities in these fluids. As yet, this MN lactate biosensor remains rather far from successful implementation *in vivo* studies despite the extraordinary reported lifetime.

More modest efforts have been invested in urea sensing (Table 4), which is considered as a biomarker for kidney and heart disorders as well as renal diseases, among others [166]. Normal concentrations of urea range from 2.5 mM to 7.5 mM and lower levels can be found in patients with hepatotoxicity (usually between 1.9 mM and 2.8 mM) [167]. Importantly, urea concentration

in ISF and blood have been demonstrated to be the same in a healthy person, which is very valuable in the search for further disease correlations [168]. Senel et al. developed an enzymatic MN urea sensor employing urease in a matrix of poly(glycidyl methacrylate-co-vinylferrocene) [128]. The attachment of urease in the MN was carried out by bringing into contact the enzyme dissolved in 10 mM PBS (pH 7.4) with the MN (previously drop-cast with polymer layer) over a period of 24 h. Calibration was performed by amperometry in artificial ISF background, and also through agarose hydrogel (phantom gel) to mimic the skin model. The LRR in both cases was the same (50–2500 μM), being adequately low to detect normal concentrations of urea in blood/ISF, whereas lower sensitivities were observed when calibration was performed through the phantom gel (31 nA mM^{-1} *vs* 52 nA mM^{-1} without the gel). The authors speculated that this decrease in sensitivity is likely attributed to the slow diffusion of urea through the hydrogel matrix. This conclusion indeed coincides with our own studies with MNs inserted in animal skin for potassium detection [138]. We demonstrated that when potassium ion concentration was increased in artificial ISF in contact with animal skin in which MNs were inserted, the final potassium concentration reached inside the skin (and therefore read by the MNs) were always lower than that concentration in the external ISF. This was determined to be a result of the diffusion and distribution of the ion, driven by the concentration gradient at the skin-artificial ISF interface, as was demonstrated by regular diffusion experiments [138]. Although it is obvious that the sensor reported by Senel et al. is not yet suitable for *in vivo* assays, this work deserves great praise for innovation in urea sensing *via* MNs [128].

An alcohol MN biosensor was introduced by Mohan et al. through the immobilization of alcohol oxidase (AOx) in a chitosan layer covered by Nafion and integrated inside a hollow polymeric MN [34]. The amperometric calibration was performed in 0.1 M PB (pH 7) and artificial ISF. The resulting LRR ranged from 0 to 80 mM in both media, which is wide enough to detect the legal limits for driving established by many countries. Interferent studies for uric acid, acetaminophen (paracetamol), and ascorbic acid were also accomplished. A signal variation of only 6% was observed during the assays using a relatively high concentration (100 μM) of such compounds. *Ex vivo* assays were performed by inserting the MN sensors in a layer of mouse skin and immersing it in artificial ISF. No structural or mechanical damage was observed in the MNs after multiple insertions and the analytical performance of the enzymatic layer was not affected by the insertion and/or biofouling either. It was claimed in the paper that the polymeric cover protected the sensor hosted inside, making it suitable for alcohol monitoring in *ex vivo* conditions. Certainly, the monitoring of ISF alcohol is a very interesting topic that could help to prevent car accidents, with sensors communicating the results directly to a smart interface placed within the car. However, it should be noted that less invasive approaches to this problem, such as sweat sensors in the gearshift and facial monitoring systems among others, are already being considered by some of the major automobile companies [169].

A similar approach was applied by Goud et al. for levodopa monitoring in ISF [106]. At the time of writing, levodopa is one of the most effective drugs for the treatment of Parkinson's disease but the dose needs to be carefully controlled depending on the symptoms of the patient [170]. Thus, if the amount supplied is too low, symptoms such as Parkinsonism and anxiety/depression may appear. Contrarily, high amounts can provoke dyskinesias, psychosis, etc. Therefore, a more reliable procedure guided by sensors could lead to an improvement in the health and quality of life of patients suffering from Parkinson's disease. The approach reported by Goud et al. uses tyrosinase to convert levodopa into dopaquinone in an electrochemically controlled reaction [106]. Tyrosinase was mixed with a carbon paste and then, hollow MNs were filled with the resulting mixture and externally covered with a protective Nafion layer. The enzymatic sensor was calibrated in artificial ISF, obtaining 0.25 μM and 0.25–3.0 μM as LOD and LRR respectively. Phantom gel based as well as *ex vivo* mouse skin assays were performed in artificial ISF media, obtaining comparable results in the LRR before and after the insertion of the MNs. Similarly to the work presented by Mohan et al., the mouseskin layer was pierced by the MNs with subsequent immersion in artificial ISF [34]. Also, with this set up, biofouling issues were evaluated using common proteins found in ISF such as albumin and γ -globulin, observing a relatively stable signal with *ca.* 11–14% of signal change (i.e. drift) over 2 h. The observed relatively low susceptibility to biofouling was attributed to the external Nafion layer.

Amperometry remains the most popular electrochemical technique in enzymatic sensors, however potentiometric approaches can also be used for biomolecule and drug detection. In this direction, Gowers et al. developed a potentiometric MN sensor for the determination of β-lactam antibiotics (such as penicillin G) [148]. As a general approach, monitoring of antibiotics with MN (bio) sensors may provide the needed information to dynamically adjust the dose for the patient. The principle of the sensor has its roots in the β-lactamase hydrolyzation of β-lactam antibiotics, which involves changes of pH in the medium. Therefore, a pH sensor can be used for the indirect determination of the antibiotic concentration. To fabricate the pH sensor, the authors deposited a film of IrOx as pH sensitive layer on the surface of a gold-covered polycarbonate MN array and then, the MNs were coated with a hydrogel containing the enzyme and an outer layer of poly(ethylenimine), which seems to enhance the stability of the sensor. Finally, the MNs were sterilized by exposure to gamma radiation.

Penicillin G calibration was performed in 10 mM PBS, resulting in a LOD of 6.8 μM, which is not low enough for most clinical purposes: peak serum levels after a 500 mg dose have been reported to be 4.4–8.1 μM and 1.8–3.0 μM for the total and free penicillin G respectively [171]. Stability studies performed for 14 days showed an initial decrease in the sensitivity during days 1–3 and a stabilization of the signal afterwards. However, it seems that the sterilization procedure negatively affects the observed sensitivity, this fact was also pointed out by other authors [102]. Interestingly, preliminary *in vivo* assays involving a healthy human volunteer were also accomplished. A calibration was performed before and after the *in vivo* insertion, and the similar values obtained demonstrated that the sensing layers were not affected by the *in vivo* measurements. Furthermore, promising results were achieved through the comparison of the values obtained with ISF collected through microdialysis measurements (requiring subcutaneous insertion of microdialysis probes) and discrete blood samples, observing the same qualitative trend over time in each case. A key aspect is the successful monitoring of penicillin in both *ex vivo* (human skin) and *in vivo* conditions. Nevertheless, the concentrations found were very similar to the LOD of the MN sensor and thus, further fundamental studies would be necessary to push down this limit in order to provide enhanced accuracy of the results, as the authors highlighted in the conclusions of their paper.

3.2. Non-enzymatic sensors

Non-enzymatic MN sensors have been reported for the detection of biomolecules, drugs, pH, ions, hydrogen peroxide, oxygen, and nitric oxide (see Table 4). In particular, some of these examples have sought to resolve the drawbacks reported for enzymatic MN glucose sensors [26,32], arising from the presence of the biological

recognition element, which includes lack of stability (enzymes are easily affected by temperature, pH, and humidity), complex fabrication procedures, oxygen limitation, economical affordability of the entire sensor and/or lack of reproducibility in sensitivity [172]. In addition, the easier fabrication process of non-enzymatic sensors could facilitate mass-production of MN sensors and their higher stability would allow for implantable probes. Besides that, acceptable analytical parameters have been reported for *in vitro* assays, such as a wide enough linear response for glucose detection in undiluted blood and ISF, with no *in vivo* analysis being attempted yet [26,32]. The detection principle omits the use of any enzyme, and the direct oxidation of glucose on platinum-based nanomaterials is used instead.

The detection of hydrogen peroxide, which is involved in many biological processes and may provide information regarding cell or DNA damage, has also been reported for non-enzymatic MNs using amperometry or cyclic voltammetry (see Table 4). The sensor fabrication procedure is commonly based on the use of noble metals (such as platinum and palladium), given the electrocatalytic activity for redox reactions of hydrogen peroxide presented by these metals [124]. Hybrid nanomaterials in which 2D graphene or molybdenum disulfide are used to immobilize NPs of precious metal have been proposed to enhance the MN sensitivity and analytical performance [124,153]. However, for the implementation of MN sensors in continuous H_2O_2 monitoring, the LRR presented by state-of-the-art MN sensors ought to be wider still, especially regarding the lower limit (and the related limit of detection). Notably, most of the reported MN sensors are not suitable for quantification of cytotoxic levels ($\geq$50 μM) [173]. Sensors of this kind can be used for the indirect determination of biomolecules whose oxidations are catalyzed by oxidases (e.g., glucose, lactate, uric acid or cholesterol), thereby avoiding the use of Prussian blue or other redox mediators [174].

Amperometric and voltammetric MN sensors have been proposed for the determination of biomolecules commonly present in ISF and blood, including ascorbic acid [122,125], uric acid [130,141] and dopamine [141], as well as potential disease biomarkers such as nitric oxide [123,144]. Because most of these biomolecules present similar anodic potentials, voltammetric sensors seem to present greater discrimination capabilities than amperometric ones, but still the presence of overlapping peaks may hinder the selective determination of a given analyte. On the other hand, MN sensors for nitric oxide detection are slightly further advanced towards *in vivo* analysis. For example, Keum et al. reported on polycaprolactone needles functionalized with hemin that are able to differentiate between melanoma tissues and normal ones [123]. Other interesting applications are the label-free quantification of DNA [126] and the monitoring of specific drugs, such as propranolol [133] or fentanyl [105].

Regarding potentiometric detection, some successful examples used MNs based on metal oxides [73,136,137] or pH-sensitive conducting polymers [155] for the determination of pH, and ion-selective membranes for the determination of potassium [111,138] and copper [156]. In particular for pH sensing, the work by Zuliani et al. used iridium oxide electrodeposited on an array of plastic MNs, enabling a mapping of pH distribution in soft and heterogeneous samples (e.g. tissues and organs) [137]. The authors stressed that the sensor was not affected by proteins such as albumin but some interference was noted with $CaCl_2$ and $MgCl_2$. The sensor was applied to cardiac tissue (rat heart) during *ex vivo* assays. pH was measured during cycles of ischemia/reperfusion events and a pH map was constructed using the values obtained from each needle of the array. However, the selectivity of the MN-based pH sensor must needs be improved, and the insertion protocol (in the tissue/organ) must be revised to avoid artifacts during the measurements due to movement of the organs, as the authors indeed indicated in that paper.

In vivo potentiometric applications have been reported only for pH monitoring in rats, specifically in brain and bladder [73,155], despite the determination of other ions being also relevant because electrolyte imbalances are associated with diverse dysfunctions and diseases, such as hypo- and hyper-natremia, hypo- and hyperkalemia, heart disorders, muscle activity deterioration, disturbances in cerebral metabolism and cystic fibrosis [48]. In this context, Sharifian et al. introduced a MN sensor for the determination of copper [156], which is important in specific nutritional and medicinal contexts due to its importance as cofactor for metalloproteins that modulate protein functions and/or produce critical enzymes for life [175]. Steel MNs were coated by a layer of polypyrrole doped with 8-hydroxyquinoline-5-sulfonic acid (PPy/8-HQS) by means of electropolymerization using the MN as substrate. Seemingly, PPy/8-HQS presents a significant selectivity towards Cu(II) ions. Thus, a LRR from 10^{-5} to 10^{-1} M was observed during the calibrations at pH 5, which is rather far from the required physiological pH range to translate the concept into *in vivo* measurements. In any event, the authors specifically used the MN sensor for environmental and food applications (spiked tap water and fruit juice samples).

Our group recently developed a potentiometric MN-based sensor using a multilayer structure ending in a potassium-selective membrane (i.e. carbon + transducer + potassium-selective membrane) [138]. Interestingly, the recipe for the external modification of the solid MN is analogous to regular werable ion sensors for sweat [163]. First, it was demonstrated that the use of a nanomaterial (functionalized multiwalled carbon nanotubes) as the ion-to-electron transducer layer provided a better stability, having a midterm drift of 1.4 ± 0.14 and 0.2 ± 0.08 mV h^{-1} for the sensors respectively without and with the transducer. Second, the observed LRR in artificial ISF (from $10^{-4.2}$ to $10^{-1.2}$ M) allowed for clear distinction between healthy and harmful levels of potassium in ISF. Then, no significant interference from the ISF matrix compounds (cations, glucose and urea) was incurred. In addition, *ex vivo* assays were performed by piercing a piece of chicken skin with both the WE and RE, immersing the whole system in artificial ISF solution, and then monitoring potassium concentration inside the skin after several additions of potassium into the ISF medium. Finally, cytotoxicity assays were performed by using immunofluorescence staining of two biomarkers: Hoechst for the nucleus of the fixed cells and KI-67 for proliferation behavior of the fibroblasts. The results proved that it is possible to use the sensor in continuous operation over the course of at least 24 h without inducing any risk for the patient.

3.3. Multi-analyte detection

When facing the issue of detection of multiple analytes, the typical means of address involves incorporating several WEs in combination in the MN array, each WE displaying specificity towards a given analyte. Then, the RE and CE can be used individually for each WE or all in conjunction, depending on the readout requirements. Interestingly, the option of combining both potentiometry and amperometry readouts in the same wearable device has been already demonstrated in the literature [176]. The reader should note that the twin approaches of miniaturization of the required instrumentation and wireless transmission of the outputs have been extensively investigated in the field of wearable electrochemical sensors, but not yet fully applied to MN-based devices. Thus, in the majority of the inspected works the authors limit the information provided to the connections between the readout electronics and the MN. This has been primarily achieved with

flexible leads [142], stainless steel fixed with epoxy resin [107] or with gold contacts together with silver epoxy [148]. However, there are some exceptions where the electronic part is more detailed. Kim et al. described their electronic part as a union of a micro controller unit, a miniaturized potentiostat, an analog/digital converter, a Bluetooth and a flexible lithium-ion polymer battery [134]. It is fairly self-evident that the grade of complexity of the sensing architecture increases with the increasing number of analytes.

Within the scope of MN sensors, multi-analyte detection has been predominantly applied to the simultaneous determination of glucose and lactate by way of enzymatic sensors [103,104,116], and several applications and electrode configurations have been reported to date (Table 4). Bollella et al. developed an array of externally modified MNs including one WE for lactate and one for glucose, RE (silver) and CE (gold) [116]. *In vitro* simulation of ISF monitoring was carried out by measuring glucose and lactate in artificial ISF through a chitosan/agarose hydrogel in flow conditions, demonstrating that the developed array is able to provide a stable signal for long periods of time (110 h). However, the clinical range expected for lactate lies outside of the observed LRR (10–100 μM) and furthermore, current density values for glucose did not correlate to the calibration graph accomplished in artificial ISF (not using the hydrogel setup). Unfortunately, the authors did not provide an explanation for this fatal issue.

A similar MN array, with two enzymatic WEs (external modification) sharing the CE (Ag/AgCl) and RE (Ag/AgCl) was reported by Trzebinski et al. for the simultaneous detection of glucose and lactate [103]. An epoxy-polyurethane membrane was deposited as the external layer of both WEs to prolong the LRR and decrease possible interferences by means of restrictive diffusion processes. Thus, LRR of 2–25 mM was reported for both glucose and lactate, although a closer look at the reported data reveals poor linearity for the lactate sensor, with an exponential trend in the calibration curve indicating saturation at a lower concentration than that reported in the upper limit of the LRR.

A single-needle approach was reported by Vasylieva et al. for the simultaneous determination of glucose and lactate in rat brain [104]: three different electrodes (for glucose, lactate, and control) were located inside a 3-mm long MN (Fig. 4b). The control electrode (BSA modified) was included in the MN to detect non-specific variations of the recorded current, which were later subtracted from the glucose and lactate signals. Importantly, the authors investigated cross-talking effects in the glucose and lactate sensors originating from the close proximity of the electrodes and/or the diffusion of generated hydrogen peroxide between them. As this may contribute to important errors in the calculation of the concentration of both analytes, the authors proposed placing the control electrode with BSA between the lactate and glucose sensors, maximizing the distance between them whilst also recording any possible non-specific current. In addition, micro-wells were introduced into the electrode surrounding to create a steric barrier against hydrogen peroxide diffusion out of the well.

Apart from glucose and lactate detection, other groups of analytes have also been explored with MN sensors (Table 4). Gao et al. reported on the simultaneous analysis of glucose, uric acid and cholesterol towards clinical information about metabolite imbalances involved in hypertension, hyperglycemia, hyperlipidemia and hyperuricemia diseases [36]. The three WEs were fabricated by the external modification of Au/Ti coated MNs using a layer-by-layer approach including polyaniline (PANI), Pt nanoparticles and the corresponding enzyme (GOx, uricase (UOx) or cholesterol oxidase (ChOx)). Seemingly, the introduction of PANI and Pt nanoparticles enhanced both the conductivity and catalytic activity of the MN. *In vitro* measurements were performed with a shared RE (Ag/AgCl) and CE (Pt), showing a LRR of 2–12 mM, 0.1–1.2 mM and 1–12 mM for glucose, uric acid and cholesterol respectively, all of which cover the corresponding physiological ranges in blood. No interferences were observed among these three analytes or from other common metabolites, such as ascorbic acid or bilirubin. The MNs were controlled by a programmed and portable multi-channel electrochemical analyzer that allowed the control of each of the electrochemical measurements from a tactile screen.

Mishra et al. [105] have recently reported an array of voltammetric sensors based on hollow MNs filled with carbon paste that is able to discriminate between episodes of opioid overdose and nerve agent poisoning. A non-enzymatic MN sensor is used to detect fentanyl (the dominant synthetic opioid) based on the oxidative dealkylation of its piperidine tertiary amine group, which results in a voltammetric peak at *ca.* 0.7 V. Then, a second electrode is modified with organophosphorus hydrolase (OPH) to detect methyl paraoxon (MPOx). This last detection is based on the indirect determination of the *p*-nitrophenol generated through the hydrolyzation of MPOx by OPH, with a LOD of 10 μM. The fentanyl sensor presented a LRR of 10–200 μM, but also, it detects morphine (20–140 μM) and norfentanyl (40–400 μM), which is the primary metabolic product of fentanyl. The discrimination between fentanyl and these other two compounds was made possible by their distinct profiles in square wave voltammetry. On the other hand, it was demonstrated that the LOD for fentanyl could be lowered down to 50 nM through the incorporation of CNTs into the carbon paste and the addition of a hybrid film comprising Au nanoparticles and electrochemically reduced graphene oxide. This decrease in the LOD is particularly important because blood fentanyl levels above 60 nM may cause fatal effects in patients [105]. This work uses an approach of separate MNs for each electrode with both WEs being connected to the same RE (Ag/AgCl wire inserted inside the MN) and CE (non-modified carbon paste), which seems to help eliminate cross-talking effects. The potential of the developed array for further *in vivo* measurements was evaluated by means of an agarose tissue-mimicking phantom gel and artificial ISF. Well-defined voltammetric peaks that increased linearly with the analyte concentration were achieved, although noticeable differences in peak potential and intensity were found compared to regular calibration curves.

Interestingly, other devices have been reported for multi-analyte sensing with MNs that are not the sensing element itself, but still playing an important role in the entire conception of the analysis. For example, Miller et al. proposed the simultaneous determination of glucose, lactate and pH using hollow MNs to drain ISF from the subject leading to external sensors located along a platform based on a flexible flat cable [112]. This device demonstrated adequate *in vitro* performance, achieving the LRR of 2–12 mM for glucose and lactate in a pH range between 5 and 8. Unfortunately, the authors did not demonstrate any implementation in *in vivo* ISF measurements.

4. Beyond the lab: challenges in real life applications and current market state

Among all the MN (bio)sensors reported in the literature in the last decade, *in vivo* applicability has been achieved in only a few cases [16,28,134,142]. In the vast majority of the published papers, the MN sensing technology remains at the laboratory scale (equivalent to TRL3, Technological Readiness Level, as defined in Horizon 2020 European guidelines), approximately halfway

towards the final goal of usability in real scenarios (at least TRL6). This last section of the review includes a discussion of the most advanced sensors that have gone through this crucial step of technological readiness; daring to perform *in vivo* measurements. An overview of the current market of monitoring with MN sensors is presented as well.

4.1. Establishing an adequate MN scheme

Table 5 lists MN (bio)sensors that have been applied to *in vivo* studies essentially involving the detection of glucose [16,28,95,134,142], lactate [104], hydrogen peroxide [124], penicillin [148], methyl paraoxon [107] and nitric oxide in ISF [123]; phenoxymethylpenicillin in ECF [157], glucose (with surgery) [140] and oxygen in blood [149]; and pH in CSF, heart and bladder, mainly in humans, rats and mice [73,137]. Attending first to the measuring scheme, two main trends are found among the collected *in vivo* studies, which are outlined in Fig. 6: direct transdermal detection, or analyte extraction through the MNs coupled to different analytical approaches.

The most common path involves the direct insertion of a MN patch in which the modified MNs are inserted and fixed at the required length to reach the fluid to be analyzed (Fig. 6a). MNs can be modified externally (Fig. 6b) or internally (Fig. 6c) with different approaches before or after being embedded in the patch. The selection of this procedure depends on the entire process of the sensor preparation and its compatibility with the patch/base material. Evidently, the final architecture must assure that the MNs resist transdermal penetration.

In this sense, several approaches have been exploited for the modification of MNs already embedded in the patch. Rawson et al. metallized polycarbonate MN arrays using chromium and a layer of gold and silver, respectively, for the WE and RE [157]. Subsequently, the WE was modified with the sensing element (β-lactamase). Samavat et al. used tetrathiafulvalene and GOx on the WEs of the MN array by spray deposition [16]. Kim et al. screen-printed carbon and Ag/AgCl layers as WE and RE in polyethylene terephthalate (PET) MNs [134]. Afterwards, an electron transfer mediator and the recognition element were electrodeposited, namely ferrocene carboxylic acid and GOx respectively. Finally, in order to protect and improve the robustness of the sensor, a mussel protein (dopa-incorporated foot protein-3) was electrodeposited on top of the WE. Jin et al. also proposed the protection of the MN sensor during insertion [124]. The authors employed Pt nanoparticles with reduced graphene deposited by dip coating to prepare the WE, followed by protection of the sensor using a water-soluble layer of polyvinylpyrrolidone (PVP). This layer ensured a safe insertion for the sensor, and a proper determination of hydrogen peroxide after the dissolution of the PVP in the subcutaneous ISF. This kind of protection approaches results interesting for MN (bio)sensors prepared as per external modification (Fig. 6b).

In contrast, greater protection during the insertion can be achieved by hosting the sensing element inside hollow MNs (Fig. 6c). Once transdermal penetration is completed, two options are possible: (i) the biological fluid will flood the inner part of the MN closing the electrochemical cell circuit for adequate readout; and (ii) the sensing element is located at the tip of the needle and is somehow in direct contact with the fluid. For example, Ribet et al. presented hollow silicon MNs that were employed as platform to include the electrodes inside their lumen (the bore at the tip of the MN) [28]. The WE and RE were made by deposition of a platinum and iridium layer respectively, following a functionalization of the WE with the sensing element (mixture of GOx, BSA and glutaraldehyde) by drop-casting means. Mishra et al. proposed filling the inner part of hollow MN with conductive inks: carbon and Ag/AgCl for the WE and RE respectively [107]. Then, the corresponding enzyme mixture for MPOx detection was deposited by drop-casting. In another approach, Vasylieva et al. used Silicon/SU8 MN to prepare MNs with micro-well structure, which were filled with GOx and LOx mixed with crosslinking agents, namely glutaraldehyde and poly (ethylene glycol) diglycidyl ether (PEGDE) [104].

MN patches have also been reported for off-body measurements based on using the MNs as fluid collectors, as illustrated in Fig. 6d and e. Accordingly, simple extraction of ISF using the MNs is possible; external analysis may then be provided by means of coupled electrodes (Fig. 6d) or centralized instrumentation (Fig. 6e), i.e. traditional analytical instrumentation placed in the laboratory (such as liquid chromatography [79] and optical sensing [177], among others). Evidently, these latter analyses do not formally pertain to wearable MN (bio)sensing technology. However, these approaches deserve special attention with regards to effective solutions for the validation of pure on-body measurements with MN (bio)sensors. For example, Miller et al. used a setup consisting of MN coupled to a glass capillary to collect the ISF [79]. Seemingly, a flow of ISF was obtained for 10–15 min following a delay of 30–120 s after insertion of the MN. Additionally, the authors established that the ISF flow was not due to capillary effects, but to the local pressure induced by the unique concentric geometry of the MN. By using this approach, no additional equipment (vacuum pump for example) were required for ISF collection.

Another approach consists of the enrichment of the MNs with the target analyte during the skin insertion. Zhang et al. described a methodology using MNs containing photonic crystal barcodes with immobilized antibody probes, which were able to selectively capture three inflammatory cytokenes (TNF-α, IL-1β, and IL-6) [177]. Once captured, the complexed cytokenes reacted with fresh antibodies in a typical sandwich immunocomplexes assay and were measured by fluorescence. Similarly, Caffarel-Salvador et al. reported on hydrogel-based MNs prepared from crosslinked poly(methylvinylether-comaleic acid) [178]. When dry, these MNs are able to easily penetrate the skin and, once inside, the hydrogel absorbs moisture from the ISF and swells, allowing substances present in the ISF to permeate into the MNs. After removal from the MN, all the accumulated substances can be measured by conventional analytical techniques. In this case, theophylline and caffeine were analyzed by liquid chromatography with UV detection whereas glucose was measured by means of a commercial glucometer.

The last measuring scheme option involves the so-called on-line measurements (Fig. 6d). MNs are used to sample ISF towards the sensing platform, which is located in the same patch that contains the MNs. Conveniently, some derivatization/pre-treatment procedures can be performed inside the MNs prior to reaching the sensing platform. An example of this approach was reported by Yang et al., who combined reverse iontophoresis and MNs to capture Epstein-Barr virus cell-free DNA (an important biomarker of nasopharyngeal carcinoma), which was directly analyzed by means of a voltammetric microfluidic-based biosensor based on recombinase polymerase amplification [179]. Thus, hydrogel-based MNs were able to isolate DNA from the epidermis in a minimally invasive manner thanks to the material of the MN (polymethyl vinyl ether-alt-maleic hydrogel), which can capture and absorb DNA. The microfluidic chip employed consisted of a two-layer structure joined by plasma treatment: a microelectrode layer and a flow channel layer. The microelectrode part included the WE (gold wire), RE (Ag/AgCl) and CE (Pt wire). The microfluidic chip was nourished by a mini-springe pump with a flow rate of 7.5 μL min^{-1}. Despite the advantages provided with this measurement scheme, problems related to the reliability of ISF extraction or a time delay associated

Table 5
In vivo and *ex vivo* applications of electrochemical MN sensors.

MN description	Analysis	Application	Measuring scheme	Monitoring time	Calibration method	Validation method	Ref
Hollow: Silicon	Glucose in ISF	Diabetic human volunteers	*In vivo*	72 h	Calibration against reference blood glucose value	Comparison with finger-pricked blood analyzed by commercial device	[95,142]
Solid: PET functionalized with GOx	Glucose in ISF	Diabetic beagle dogs, monkey and human volunteers	*In vivo*	5 days (dogs) 3 days (human)	NS	Blood sampling and analysis by reference device (Accu-check Performa)	[134]
Solid-coated: SU8 coated with C and functionalized with GOx	Glucose in ISF	Healthy human volunteers	*In vivo*	3 h	NS	Comparison with finger-pricked blood analyzed by commercial device	[16]
Hollow: Silicon functionalized with GOx	Glucose in ISF	Healthy human volunteers	*In vivo*	90 min	NS	Comparison with finger-pricked blood analyzed by commercial device	[28]
Solid-coated: Polycarbonate coated with Pt and functionalized with GOx	Glucose in ISF	Healthy and diabetic human volunteers	*In vivo*	24 h	Calibration against blood values 2 h after insertion. External calibration post-removal	Blood sampling and analysis by reference laboratory method (YSF glucose analyzer)	[147]
Solid-coated: SST coated with AuNP/PtNP and functionalized with GOx	Glucose in blood	Anesthetized male mice	*In vivo*	3 h	Calibration in PBS after on-body measurements	Blood sampling and analysis by glucose testing strips	[140]
Solid: SU8 functionalized with GOx or LOx	Glucose and lactate in ISBF	Anesthetized male rats	*In vivo*	3 h	Calibration in PBS before and after on-body measurement	No validation	[104]
Solid-coated: β-lactamase functionalized MN	Phenoxymethylpenicillin in ECF	Healthy human volunteers	*In vivo*	6 h	Plotting of random timepoints against microdialysis data	ECF is extracted by microdialysis and analyzed by HPLC-MS	[157]
Solid-coated: Polycarbonate coated with Cr/AU and functionalized with β-lactamase	Penicillin in ISF	Healthy human volunteers	*In vivo*	6 h	Calibration in PBS before and after on-body measurement	ECF is extracted by microdialysis and analyzed by HPLC-MS	[148]
Solid-coated: PCL coated with PEDOT and functionalized with hemin	Nitric oxide in ISF	Anesthetized healthy and melanoma mice	*In vivo/Ex vivo*	5 min	No calibration	Confirmation of melanoma diagnosis through endomicroscopy	[123]
Solid coated: W coated with ZnO	pH in CSF and bladder	Anesthetized female mice	*In vivo*	60 s	External calibration in buffer	CSF and bladder urine collection and analysis by portable pH-meter	[73]
Solid-coated: SST coated with Pt/rGO	H_2O_2 in ISF	Pig skin Living mice	*Ex vivo/In vivo*	90 s 400 s	External calibration in PBS	Skin tissues are minced and quantified with H_2O_2 kit	[124]
Hollow-pyramidal: Filled with carbon paste containing OPH	MPOx in ISF	Mice skin	*Ex vivo*	30 s	External calibration in artificial ISF	Exposing mice skin to MPOx and calculating recoveries	[107]
Solid-coated: PET coated with Au/IrOx	pH in heart	Explanted hearts from male rats	*Ex vivo*	70 min	External calibration: 2 points in buffer and 1 point in Tyrode's solution with the heart, last point repeated post-removal	No validation	[137]

COC: cyclic olefin copolymer; CSF: cerebrospinal fluid; ECF: extracellular fluid; GOx: glucose oxidase; ISBF: interstitial brain fluid; ISF: interstitial fluid; LOx: lactate oxidase; MPOx: methyl paraoxon; NP: nanoparticle; NS: not specified; OPH: organophosphorus hydrolase; PCL: polycarprolactone; PEDOT: poly(3,4-ethylenedioxythiophene); PET: polyethylene terephthalate; SST: stainless steel.

to the analyte diffusion from ISF to the sensing platform have been claimed in the literature [179].

4.2. Particular and traditional analytical requirements for MN (bio) sensors

Major challenges to reliable *in vivo* analysis are found in the proper calibration and validation of the MN (bio)sensors. In fact, most of the works reported in the last decade have been limited to the monitoring of analyte changes, not being able to provide a validated quantification. In the case of glucose, as the main compound analyzed with MN-based measurements, some authors have proposed the calibration of glucose MN sensors against the values obtained in blood [95,142,147]. Random intensity values (from amperometry measurements) obtained in ISF are plotted against blood concentration (from glucometer measurements), at the corresponding time, in order to calibrate the sensors. Nevertheless, this procedure should be avoided because it may provide biased results that do not consider concentration differences between simultaneous measurements in ISF and blood due to the

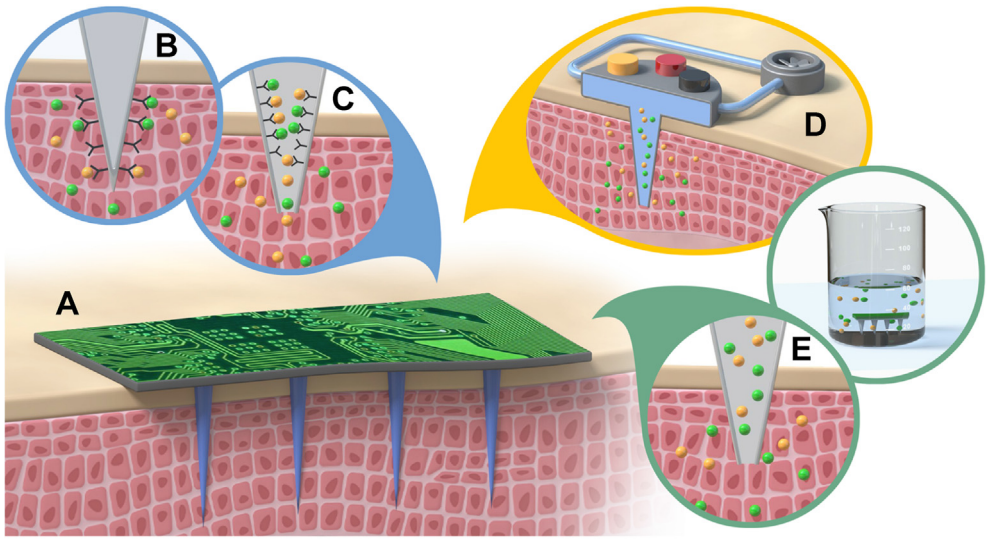

Fig. 6. Scheme of most common approaches in the employment of MN sensors: A) a MN sensor patch placed on human skin, B) on-body MN sensor based on external modification, C) on-body MN based on internal modification, D) online MN sensor and E) off-body measurements using MN.

above-mentioned diffusion issues. In addition, this sort of calibration would be valid only for glucose, and perhaps lactate with the use of the lactometer, but it is not a general protocol for calibration (and neither for validation) of ISF (or other) *in vivo* measurements.

Any protocol generally involves the calibration of the MN sensors before and after the *in vivo* application. Besides obvious quantification purposes, this double calibration allows one to evaluate any effect of the skin penetration process in the sensor response. Also, this double calibration may help to correct drifts and assess biofouling processes [104,157]. Thus, with optimal accuracy as the intention, it is crucial to select appropriate calibration conditions in terms of number of datapoints, background, and set up. For example, some authors have performed external calibrations in buffer solution rather than using the artificial version of the corresponding biological fluid [73,124]. Although this practice could be claimed to be an adequate alternative in the case of ISF because of its simplicity compared to blood, ISF still contains different ions and some small organic molecules (such as sodium, magnesium, calcium, CO_2, glucose and albumin) that can result in a matrix effect in the sensor response [85].

Maintenance of the calibration parameters of MN (bio)sensors after skin insertion has been generally considered in the literature as a sign of robustness and reliability of the external calibration in quantifying analyte concentrations [104,148]. In this case, a threshold value should be set to establish the accepted difference in the parameters before and after calibration. Vasylieva et al. set the threshold for the slope (or sensitivity) at 40% [104]. However, considering that their aim was the development of a medical device for health evaluation, a more discrete threshold of <20% (as in the case of commercially available glucometers) would be a more suitable value to further pursue *in vivo* measurements. Indeed, it is evident that this approach can only guarantee that MN sensors are not affected or altered during *in vivo* measurements because of the insertion process). Overall, the calibration protocol evidently remains controversial in wearable MN technology.

In one particular case, MN sensors have been used to confirm the presence of the analyte without the need for a calibration graph to quantify its concentration. Keum et al. developed a MN sensor to monitor melanoma *via* concentration of nitric oxide in the colon of mice [123]. The MNs were placed at the end of an endomicroscope, which additionally served to collect polyps. The main indicator of the presence of cancer was a change in the current recorded by the MNs due to the increase of nitric oxide (produced by nitric oxide synthase in the cancerous region), such that an exact value of its concentration was not required and, therefore, calibration was not necessary. The validation step was performed by using a biopsy of the polyp region [123].

Apart from this specific example, finding a suitable calibration protocol for each particular analyte is a challenge, mainly due to the difficulty in translating *in vivo* conditions to an *in vitro* set up, in addition to alterations that the sensor could experience during skin penetration or the *in vivo* measurement *per se*. Hydrodynamics or changes in mass transport conditions can impact also on the sensor response [148]. Up to this point, traditional calibration protocols have been adapted to the special conditions required for reliable ISF analysis with MNs. For example, Zuliani et al. impressively monitored the pH in a mouse's heart immersed in a Tyrode solution (isotonic solution based on ISF matrix) over ischemia/reperfusion episodes [137]. For this purpose, a two-point calibration was performed before the *ex vivo* experiment to find the slope in buffer solutions and a one-point calibration was performed in the Tyrode solution to adjust the offset, assuming that the slope of the calibration graph was not altered. This last calibration point was repeated after each ischemia/reperfusion assay. It was demonstrated that the offset was linearly changing over time, and accordingly, drift corrections were accomplished.

Regarding the validation strategy, and returning to the case of glucose, most of the reported MNs analyzed either ISF or blood, and used a validation method that involves blood glucose analyses with commercial glucometers. In the case of ISF analysis, this validation approach evidently assumes equal concentration of glucose in ISF and blood, setting aside the fact that the veracity of this assumption is time-dependent, as already illustrated in previous sections. While this approach could not even be considered a pure validation protocol (because the two techniques which are compared do not consider the same biological fluid), it allows for an approximated comparison between blood and ISF glucose pursuing reliable correlation studies. This method is of course totally acceptable for glucose analysis in blood.

In principal, validation strategies should be based on the extraction of the targeted body fluid. To this end, finger pricking,

aspiration and microdialysis have been reported [82,146,157]. Rawson et al. determined penicillin in extracellular fluid and the results were validated using microdialysis to extract serum samples, which were later analyzed by high performance liquid chromatography coupled to mass spectrometry [157]. It was possible to observe similarities between the time-profiles obtained with the MN device and the gold standard technique, indicating a suitable on-body monitoring of the drug with MNs. Mani et al. used MN sensors to measure pH in brain and bladder samples obtained from mice with a validation protocol involving the extraction of cerebrospinal fluid and urine by means of aspiration through a 33-gauge needle attached to a polyurethane tube and inserted into the brain and bladder [73]. Then, the samples were analyzed with a commercial pH meter. The values obtained were always higher in the case of the commercial pH meter. Hence, the authors assumed that pH changes could occur simply upon extraction of the fluid from the mouse body. These results indeed accentuate a reasonable explanation for the lack of validation protocols in ISF measurements with MNs, this being the lack of reliable methods for extraction or collection of the ISF volume needed for analysis with a gold standard technique.

Concerning lifetime requirements to address *in vivo* measurements, one of the advantages of using MN sensors is the possibility for real-time, continuous monitoring, which can facilitate the daily monitoring of ill people in the clinical field. In addition, considering the options beyond punctual clinical measurements, it is important to evaluate the resiliency of the MN sensors facing certain corporal movements. This is in turn significant toward possible applications in assessment of sport performance. On the one hand, few *in vivo* studies have been carried out for periods longer than 24 h [95,134,142,147] to demonstrate the long-term suitability of the technology: a good practice could be based on disposable patches that can be replaced every 24 h (or any other time frame). On the other hand, there is a lack of information about resiliency studies and the manner in which corporal movement affects MN sensors during *in vivo* assays, whereas this sort of assay has been successfully addressed in previous steps (*ex vivo* conditions). For example, Ciui et al. explored the consequences of twisting and bending repetitively a tyrosinase MN sensor on the recorded signal [37].

Toxicity-related experiments are also essential towards *in vivo* demonstration of MN sensor operation, which may limit the wearable lifetime of the MN patch. Even if this topic seems obvious, unexpected lack of information can be appreciated in the literature involving *in vivo* assays, with the majority of the works only mentioning the use of biocompatible materials (such as ZnO [73], IrO_2 [148], silicon substrates [95,104] and mussel protein [134], among others) but not performing pure cytotoxicity assays. Contrarily, other authors employ substances which cannot clearly be considered non-toxic (e.g., tetrathiafulvalene [16] and organophosphorus hydrolase [107]). In the cases where not all substances/materials are entirely biocompatible, it is important to be able to prove that there is no risk for human health during the entire employment of the device. For this purpose, two main circumstances must be confirmed: (i) no leaking of any substance during the use of the device, and (ii) the corresponding cytotoxicity assays indicating that skin (or tissue) cells are not negatively affected by contact with the sensor. In this context, our previous work with potentiometric MNs for potassium can be highlighted as a suitable example [138], together with our recent paper about cytotoxicity studies involving ionophore-based membranes regularly used in potentiometric sensing of ions [143]. Owing to these studies, it is possible to establish limits for the continuous use of the MN (bio) sensors without compromising the patient's health (for example, at least 24 h with MNs for the potentiometric detection of potassium) [138,143].

Despite positive results arising in cytotoxicity studies, this is not enough to obtain the medical approval for the studies required prior to market commercialization. The MN device must additionally adhere to the regulations for medical devices (legislatives rules), which are for example established by the United States Federal Food and Drug Administration (U.S. FDA) in the USA, and the European Union Medical Device directive in the EU. For each new product, a standard document must be presented specifying compliance to the rules and guidelines as well as providing the instructions for its use in a certain environment, alongside the results demonstrating the quality of the product. This document should be in alignment to the corresponding International Organization for Standardization (ISO) standard: mainly, ISO 9001, for the business part and ISO 13845 for the issues related with medical devices [180]. On-body measurements should also consider the ISO 10993 series, which establishes necessary assays such as genotoxicity, cytotoxicity, local effects after implantation, intradermal reactivity, sensitization as well as systemic and acute systemic toxicity to ensure that the medical device is safe for humans during testing procedures.

4.3. Analyzing particular examples demonstrated for in vivo analysis with MNs

Among all the MN (bio)sensors reported in the literature in the last decade, only 12 have been demonstrated for *in vivo* applications. Jina et al. used a patch based on an array of hollow MNs to extract ISF towards Pt WEs modified with GOx and BSA for on-line determination of glucose [142]. The authors set four of these devices in the upper arm and forearm of 10 diabetic human subjects (seven were of type 1 and three of type 2) subjects to monitor glucose for 48 or 72 h. During this period, changes in glucose concentration were induced through the manipulation of insulin and diet. The system was initially calibrated using reference blood glucose values obtained by finger pricking and recalibrated once per day, which represents a lower calibration frequency than the majority of the commercially available devices. Additionally, blood reference values were measured every 20 min during daily hours for validation purposes. A lag time of 17 min (determined in a prior study with healthy volunteers) was applied to calibration and validation values to account for the diffusion time between blood and ISF. After this correction, a good correlation was observed between different devices carried out in the same subject as well as between the values from the MN sensor array and the reference fingerstick blood glucose values. The rather good correlation displayed over the entire study demonstrates the long-time operability of the developed device with only one calibration per day. On the other hand, the impact of the device on the skin in terms of irritation (erythema and edema) was also scored in a modified Draize scale (scale 0−4, with higher numbers indicating more severe irritation), showing an edema and erythema average score of 0.06 and 1.54, respectively. In all cases the damage was healed without treatment in several days.

A similar protocol was used by Samavat et al. for the *in vivo* determination of glucose using a GOx spray-coated MN sensor [16]. This device was tested with healthy volunteers, starting the recording in a fasting state and then drinking 120 mL of Polycal® complex carbohydrate drink to increase the concentration of glucose. The amperometric current was allowed to stabilize for 2 h before starting the protocol measurement and, finger prick readings were collected every 15 min for comparison purposes. Quantification was not achieved as the device was not calibrated, although the plotting of current *vs.* blood reference values revealed

a similar trend with a lag time of 20 min, which is indeed close to the value of 17 min reported by Jina et al. [142]. Interestingly, the authors explained this delay using two diffusional components, the first related to the time needed for glucose diffusion from blood vessels to ISF and the second to a limited diffusion in the epidermis that hinders the movement of ISF through the sensing layer.

Higher accuracy in glucose detection may even be achieved using algorithms that consider both temperature and time lag compensations. Kim et al. developed the corresponding algorithm by first testing their PET/GOx functionalized sensors with beagles (dogs) and monkeys (Fig. 7a and b), assuming a similar behavior in these animals as in humans [134]. Then, the device was applied to the determination of glucose in 10 diabetic (type 1) human volunteers (Fig. 7c). After stabilizing the sensor for one day, an oral glucose tolerance test (OGTT) and a meal tolerance test (MTT) were performed. In these tests, glucose concentration was altered by drinking an oral glucose sample (in OGTT) or consuming a standardized meal (in MTT), and glucose concentration was determined every 60 s with the MN sensor. Venous blood samples were collected for validation purposes before glucose intake, every 15 min during the first hour after it, and every 20 min for the next two hours. The vast majority of the data obtained with the sensor is in agreement with that procured from the venous blood measurements using a gold standard technique (YSI 2300 STAT plus), revealing a better accuracy than many commercial glucose monitoring systems. After a prolonged

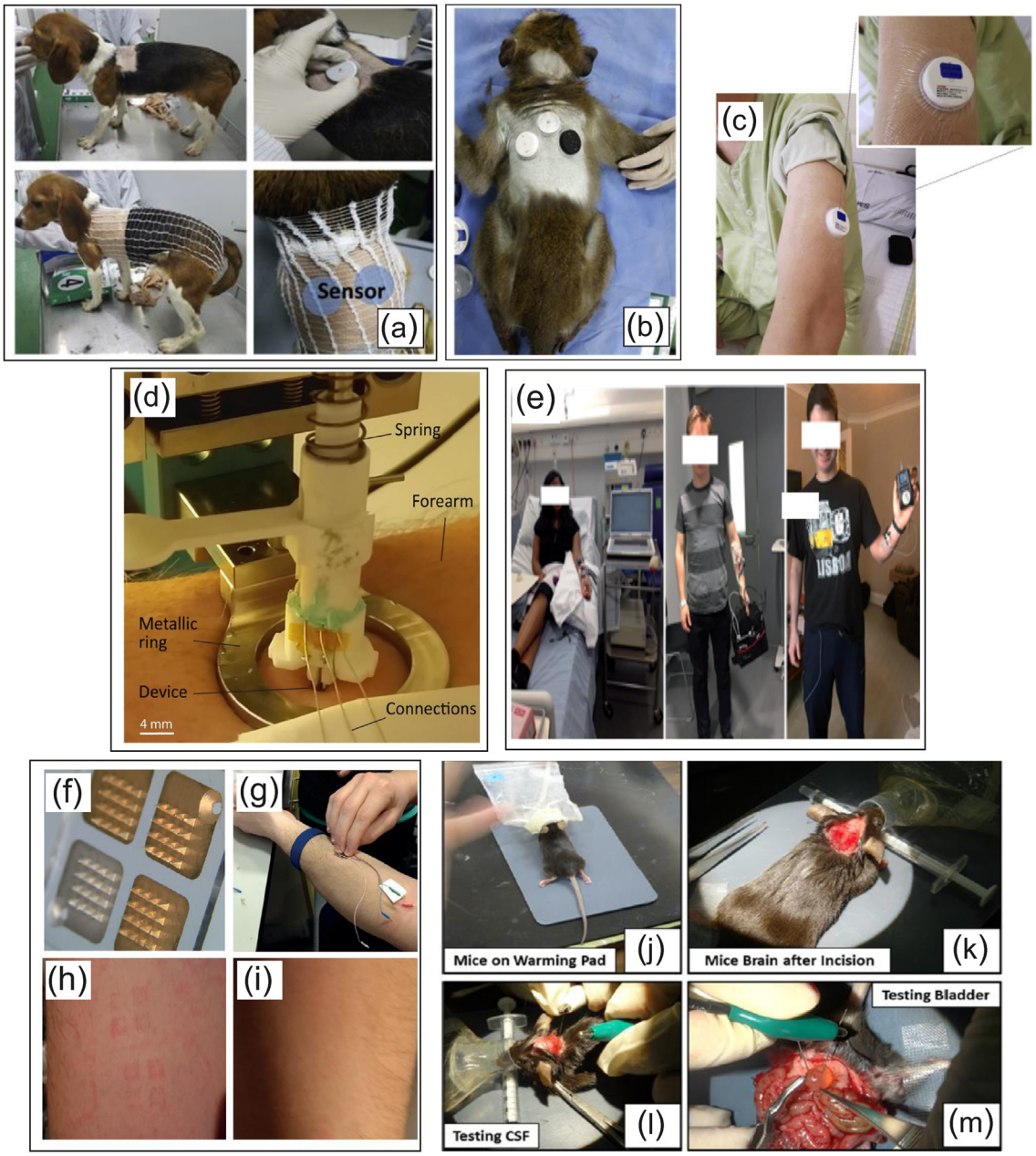

Fig. 7. Figures of *in vivo* assays: determination of glucose (a) in beagle dogs and (b) cynomolgus monkey, (c) implanted glucose MN sensors in human volunteer (Reproduced with permission from Ref. [134]), d) home-made insertion tool for the implantation of MN sensor (Reproduced with permission from Ref. [28]), e) regular and portable potentiostats employed for the determination of glucose (Reproduced with permission from Ref. [147]), f-i) MN arrays insertion and resulting skin irritation for the monitoring of phenoxymethylpenicillin penicillin in human (Reproduced with permission from Ref. [157]), (j-m) determination of pH in rat brain (Reproduced with permission from Ref [73]).

sensor attachment, no sever skin irritation was produced, although in some cases red traces in the zone where the sensor was attached could be observed. These traces disappeared during the following 3 days.

The system employed in order to perform the insertion of MNs into the skin is an important aspect which has not been very frequently addressed in the literature. Ensuring a proper and deep insertion that is stable for a prolonged time can be relatively challenging due to the elastic nature of the skin. Also, insertion speed is a key factor [181]. In this context, Ribet et al. used a custom-made tool (Fig. 7d) to insert the MN device into human volunteers' forearm with a speed of 3 m s^{-1} and force of 5 N [28]. It was necessary to secure the device further using adhesive tape to maintain a suitable depth for the entire duration of the measurements. This set up provided the necessary stability for the performed measurements, but the authors suggested that a more suitable arrangement should be developed if longer analysis times (>24 h) or higher movement of the volunteers are to be considered. The monitoring of glucose over time also consisted of a glucose tolerance test with discrete finger pricked blood reference values used for validation. The values obtained with the MN device correlate well with blood reference values, taking into account a lag time of 10 min.

Probably the most complete *in vivo* study for glucose determination using MN sensors with human volunteers was performed by Sharma et al. [147]. This study involved 3 different phases. In phase 1 the glucose device (polycarbonate MNs coated with Pt, functionalized with GOx and sterilized using gamma radiation) was inserted for 6 h in 8 healthy volunteers to check their level of tolerance for MN arrays. After this time, the device was removed from the skin and the patient scored the sensation of pain according to the so-called Visual Analogue Scale. The median score for the pain was 10, much lower than that associated with the insertion of an intravenous cannula (score of 30). Phase 2 involved the insertion of the device in healthy volunteers for 24 h and was aimed to investigate both the depth of penetration and any movements or dislodgements that occurred during this period. A non-invasive imaging technique (Optical Coherence Tomography) was employed to evaluate the insertion performed in each case, revealing that the insertion depth remained constant over the 24 h testing time. Finally, Phase 3 involved 10 participants suffering from type 1 diabetes. According to the participants, the pain inflicted by the MN device was comparable to that inflicted by a commercial device for glucose detection (Dexcom G4 Platinum), but lower than the pain felt during the insertion of an intravenous cannula. In this phase, both regular and portable potentiostats were used to evaluate the performance of the MN sensors with the motion of the patient (Fig. 7e). Although the MN measurements lasted for 24 h, the portable potentiostat encountered issues in maintaining electrical connection at night; therefore, only day measurements were evaluated. For comparison purposes, venous blood was sampled every 30 min and analyzed by a reference method (YSI Glucose Analyzer). Surprisingly, the obtained data did not present a constant lag time, with results ranging between 0 and 15 min. Clarke error grid analysis was applied for the comparison of MN sensors and blood reference values, showing that 96.4% of the data fell within the clinically acceptable zone, which proves the feasibility of the MN device.

Other authors have reported the *in vivo* determination of glucose in anesthetized rats/mice, which are usually employed as a first step in proof-of-viability studies for sensors in real clinical contexts. Chen et al. implanted their sensor close to the spinal cord of anesthetized rats and secured it using a plastic adapter with electrical connections [140]. Glucose concentration in ISF was measured for 200 min and compared to blood glucose levels obtained from tail veins *via* glucose strips. Changes in glucose concentration were induced through the intraperitoneal injection of glucose solution and a good correlation was observed between the response current and the measured blood glucose values. Particularly, an increase of 30% in glucose blood concentration corresponded to an increase of 38% in the current obtained. Alternatively, insulin was injected to decrease glucose concentration, observing a 42% and 47% decrease in blood values and sensor current, respectively. In terms of skin irritation, a minor inflammatory response was observed around the MN sensor three days after the implantation. According to the authors, the minimal level of inflammatory response is related to the high biocompatibility of the polyvinylidene fluoride Nafion coating materials.

In vivo assays with anesthetized rats were also performed by Vasylieva et al. for the simultaneous determination of glucose and lactate in the brain [104]. In this case, the electrodes were all implanted in the motor cortex of the brain, using a single probe to reduce the number of insertions and thereby avoid further brain damage. The assays lasted between 3 and 5 h, over which time insulin and glucose administration was employed to manipulate glucose concentration. Manipulation of lactate concentration was not possible due to the lack of a consensual treatment able to induce changes in lactate concentrations without impacting extracellular glucose concentrations. No validation procedure was carried out for the obtained concentration values but, according to the authors, they were in agreement with previously reported data.

Rawson et al. performed an *in vivo* assay for the determination of phenoxymethylpenicillin in human volunteers [157]. This study included 10 healthy volunteers who took a standard treatment dose for bacterial infections in adults consisting of 6 oral doses of phenoxymethylpenicillin (500 mg every 6 h). MN patches including three WE arrays (β-lactamase based biosensor) referred to the same RE (Fig. 7f) were attached to the participant's forearm with firm pressure for 60 s and secured in place with transparent medical dressing (Fig. 7g) before the final dose. MN biosensors recorded the current for up to 6 h. Blood samples and extracellular fluid were collected, *via* cannula and microdialysis respectively, at discrete times and then analyzed by liquid chromatography coupled to mass spectrometry for comparison purposes. MNs were calibrated against microdialysis data after data collection. Similar trends and values were obtained with MN sensors and the microdialysis approach. Regarding the effect of MN attachment to the participant's skin, red marks could be observed after removal of the device (Fig. 7h), which completely disappeared after 12 h (Fig. 7i).

In vivo assays at a lower temporal scale have also been carried out with animals. Jin et al. reported the *in vivo* determination of hydrogen peroxide in mice; their MN sensor setup consisted of reduced graphene oxide and Pt nanoparticles [124]. The mice were anesthetized and shaved prior to the measurement and the MN patches were placed on the back. Before starting the measurement, the sensors were left for 5 min inside the skin to allow for dissolution of a polyvinylpyrrolidone layer employed to protect the MN sensor during the insertion. In this case, changes in hydrogen peroxide concentrations were induced by subcutaneous or intraperitoneal injections of a PBS solution containing hydrogen peroxide. In the case of intraperitoneal injections, the results indicated a rapid diffusion of hydrogen peroxide from the intraperitoneal space to the local tissue near to the MNs. Additionally, the effect of the MN patch in the skin was evaluated by pressing the patch onto the mice's back for 10 min and analyzing the skin tissue after 12 h. No obvious signs of skin irritation or inflammation were observed when compared to control skin tissue.

MN based sensors have also been tested *in vivo* for disease screening using punctual measurements. Keum et al. screened colon cancer in mice using hemin modified MN sensors for the

determination of nitric oxide [123], which acts as a clinical indicator for cancer progression. For this purpose, both normal and ill mice were screened, and the increase in current observed was greater for ill mice due to increased nitric oxide concentration. This assay was carried out using a dual-diagnostic system comprising the MN sensors and an intravital endomicroscope, which allowed for the visualization (and collection) of polyps. Discrete measurements were also carried out by Mani et al. for the determination of pH in mouse brain and bladder (Fig. 7j-m) [73]. Access to these organs required surgery and measurement time was limited to 60 s to minimize the pain. Five healthy mice were included in the study and both CSF and urine were collected by aspiration for comparison purposes. Samples were immediately measured using a commercial pH meter, obtaining values slightly higher than those measured with the MN sensors.

4.4. MN sensors in the market

Despite the relatively high number of publications and the efforts devoted to creating robust and reliable MN devices with the corresponding *in vivo* studies, only a few examples have reached the market (or show promise to do so). Table 6 summarizes the current market scenario regarding MN sensors. There is a clear market niche for glucose monitoring, most probably because diabetes treatment represents a huge worldwide market that is regrettably expected to grow in the near future. In this context, MN sensors may offer the key benefit of avoiding the unpleasant process of extracting blood *via* finger pricks. In addition, continuous glucose monitoring may provide much better control and foresight to the patient, contributing to a considerable improvement in health quality and well-being.

Only some companies have put efforts into the elaboration of competitive products to satisfy this need. Dexcom [182] and Abbott [183] have bid for wireless devices, which can be controlled by the patient and/or doctor by means of a smartphone app. This approach grants a more attractive product, clearly entrenching within the minds of the costumers the idea of continuous monitoring; as at any time and in any place they could simply take a look at their smartphone screen to check their glucose level. On the other hand, both Dexcom G6 CGM [39] and FreeStyle Libre 14 days [40] systems are factory calibrated, which is a clear advantage to previous models commercialized by the same companies, as there is no need for recalibration by the end-user.

It is important to clarify that not every product sold for "continuous glucose monitoring" actually offers exactly that. For example, Medtronic [184] offers some MN products as sensors for continuous glucose monitoring, but specifies in the warnings that the data recorded is not available for the patient in real time, and that this technology is not recommended as a total replacement for conventional finger-prick blood. This clearly demonstrates the lack of viability of this device in the context of this market.

There exist other companies which, while they do not yet have any products on the market, have announced *via* their corresponding websites the pending availability of powerful alternatives for continuous glucose monitoring. For example, the website of PK Vitality [185] includes a microneedle-based smartwatch product [186]. This is an example of the company clearly following the current trend in the smartwatch market: it is already commonly possible to observe people wearing watches or bracelets that monitor physical body functions such as steps, cardiac rhythm, blood oxygen and sleeping cycles. Thus, such an analysis platform already in the minds of costumers, and the implementation of new sensors within this existing framework to evaluate more complicated biomarkers would seem the path of least resistance in order to keep ensuring profitable return from these products. In fact, PK Vitality also claims that another of their promoted products, *K'Watch Athlete* [187], will allow continuous monitoring of lactate, again offering a smartwatch as the analysis platform, and focusing heavily on an athletic or sporting target demographic. Lactate monitoring is currently not in high demand, when compared to the situation for glucose. Nevertheless, it remains highly possible that elite level athletes and their corresponding support teams would invest in such a device for the evaluation of lactate levels during training in real time. It is not difficult to imagine that a more complete control over the parameters of effort invested with respect to the performance obtained would be beneficial, as the risk of injury would be lowered. It goes without saying that injuries can be absolutely ruinous to a sporting career. Furthermore, at this top level of elite athletes, any improvement in performance whatsoever can mean the difference between success and failure, victory and defeat.

When considering commercial products intended for domestic use, thus far the only exploitation that has been undertaken (or is visibly underway) pertains to continuous monitoring of glucose and lactate. However, even in the case of glucose monitoring, despite the appreciable demand the product portfolio to choose from remains rather limited. According to the *American Diabetes Association* [188], 327 billion dollars were spent on diabetes treatment in 2018, clearly not a negligible sum. Therefore, there is a large population of diabetic people that could and would use a continuous glucose monitoring system based on MNs. In all likelihood, the existence of a well-established system which chains diabetic people to the blood finger strips in perpetuity, generating a constant money flow to the companies producing these strips, is the major braking force holding back advancements in this field. Thus, MN systems must be made more expensive in order to overcome the deficit imposed by the existing system. Above all, a clear marketing strategy must be implemented in order to convince diabetic people, who will be giving their money for these products, of their worth.

Table 6
Commercially advertised MN sensors.

Name	Company	Analyte
iPro 2 Professional CGM	Medtronic	Glucose
Dexcom G6 CGM	Dexcom	Glucose
FreeStyle Libre 14 days system	Abbott	Glucose
K'Watch Glucose[a]	PK Vitality	Glucose
K'Watch Athlete[a]	PK Vitality	Lactate

[a] No commercial device is available yet/pending medical certification.

5. Conclusions and future prospects

In the last decade considerable efforts have been directed, in the development of electrochemical MN (bio)sensors, to establishing many different approaches that integrate the sensing concept into the MN platform while aiming to inflict minimal pain on the subject. In the majority of cases, the sensing event occurs transdermally, once it has been verified that the analytical features of the sensor remain constant after the skin penetration, and that an external calibration of the sensor can serve to accurately quantify the analyte concentration. However, only very few MN devices have been used to demonstrate real *in vivo* measurements in animals and humans; the rest remain at the *in vitro* and *ex vivo* stage showing adequate performances through phantom gel and/or sectioned animal skin. Although glucose is the principal analyte targeted by electrochemical MN (bio)sensors, other species such as lactate, drug compounds, nitric oxide, pH (hydrogen ions), and other ions are gaining momentum. Thus, a shift has been noted

among the reported sensors from amperometric enzymatic detection to non-enzymatic approaches, with a view to more stable and reliable sensors. It is possible to implement all of the electrodes necessary to complete the electrochemical cell in only one MN or in distinct MNs, each approach presenting its own advantages. In addition, several works have put forward MN devices for multi-analyte detection, for example for the simultaneous detection of glucose and lactate. Regarding the assessment of the analytical features of electrochemical MN (bio)sensors, this review points out deficiencies in the protocols deployed for the calibration and validation of the sensors, together with a lack of biocompatibility (cytotoxicity and inflammation) and durability studies. These factors, together with the difficulties encountered in attaining formal approvals for *in vivo* studies, likely constitute a bottleneck for electrochemical MN (bio)sensing technology when trying to expand into the commercial market, or achieve a higher TRL. It is strongly advisable that further research in the field focuses on these aspects to fully take advantage of the great potential of MN sensors towards continuous monitoring in healthcare.

Declaration of competing interest

The authors declare that they have no known competing financial interests or personal relationships that could have appeared to influence the work reported in this paper.

Acknowledgements

We kindly acknowledge the following agencies and foundations: KTH Royal Institute of Technology (K-2017-0371), The Swedish Research Council (Project Grant VR-2017–4887), Stiftelsen Olle Engkvist Byggmästare (204-0214), Novo Nordisk Fonden (19OC0056171). In addition, we sincerely thank the fruitful discussion with clinicians/researchers from both the Medical University of Graz and Karolinska Hospital to corroborate the relevance of some analytes listed in Table 1.

References

[1] K. Mahato, A. Srivastava, P. Chandra, Paper based diagnostics for personalized health care: emerging technologies and commercial aspects, Biosens. Bioelectron. 96 (2017) 246. https://doi.org/10.1016/j.bios.2017.05.001.
[2] A. Priye, S.W. Bird, Y.K. Light, C.S. Ball, O.A. Negrete, R.J. Meagher, A smartphone-based diagnostic platform for rapid detection of Zika, chikungunya, and dengue viruses, Sci. Rep. 7 (2017) 44778. https://doi.org/10.1038/srep44778.
[3] A. Dhiman, P. Kalra, V. Bansal, J.G. Bruno, T.K. Sharma, Aptamer-based point-of-care diagnostic platforms, Sensor. Actuator. B Chem. 246 (2017) 535. https://doi.org/10.1016/j.snb.2017.02.060.
[4] G. Maduraiveeran, M. Sasidharan, V. Ganesan, Electrochemical sensor and biosensor platforms based on advanced nanomaterials for biological and biomedical applications, Biosens. Bioelectron. 103 (2018) 113. https://doi.org/10.1016/j.bios.2017.12.031.
[5] H. Xu, A. Xia, J. Luo, M. Gao, R. Liao, F. Li, Q. Zhong, W. Zhang, Y. Wang, J. Cui, W. Fu, K. Chang, M. Gan, W. Jiang, M. Chen, A sample-to-answer quantitative platform for point-of-care testing of biochemical markers in whole blood, Sensor. Actuator. B Chem. 308 (2020). https://doi.org/10.1016/j.snb.2020.127750.
[6] J. Heikenfeld, A. Jajack, J. Rogers, P. Gutruf, L. Tian, T. Pan, R. Li, M. Khine, J. Kim, J. Wang, J. Kim, Wearable sensors: modalities, challenges, and prospects, Lab Chip 18 (2018) 217. https://doi.org/10.1039/c7lc00914c.
[7] M. Parrilla, M. Cuartero, G.A. Crespo, Wearable potentiometric ion sensors, Trac. Trends Anal. Chem. 110 (2019) 303. https://doi.org/10.1016/j.trac.2018.11.024.
[8] P.C. Ferreira, V.N. Ataíde, C.L. Silva Chagas, L. Angnes, W.K. Tomazelli Coltro, T.R. Longo Cesar Paixão, W. Reis de Araujo, Wearable electrochemical sensors for forensic and clinical applications, Trends Anal. Chem. 119 (2019). https://doi.org/10.1016/j.trac.2019.115622.
[9] M. Cuartero, M. Parrilla, G.A. Crespo, Wearable potentiometric sensors for medical applications, Sensors 19 (2019). https://doi.org/10.3390/s19020363.
[10] W. Gao, G.A. Brooks, D.C. Klonoff, Wearable physiological systems and technologies for metabolic monitoring, J. Appl. Physiol. 124 (2018) 548. https://doi.org/10.1152/japplphysiol.00407.2017.
[11] S. Emaminejad, W. Gao, E. Wu, Z.A. Davies, H. Yin Yin Nyein, S. Challa, S.P. Ryan, H.M. Fahad, K. Chen, Z. Shahpar, S. Talebi, C. Milla, A. Javey, R.W. Davis, Autonomous sweat extraction and analysis applied to cystic fibrosis and glucose monitoring using a fully integrated wearable platform, Proc. Natl. Acad. Sci. U.S.A. 114 (2017) 4625. https://doi.org/10.1073/pnas.1701740114.
[12] A. Wiorek, M. Parrilla, M. Cuartero, G.A. Crespo, Epidermal patch with glucose biosensor: pH and temperature correction toward more accurate sweat analysis during sport practice, Anal. Chem. 92 (2020) 10153. https://doi.org/10.1021/acs.analchem.0c02211.
[13] J. Kim, M. Kim, M.S. Lee, K. Kim, S. Ji, Y.T. Kim, J. Park, K. Na, K.H. Bae, H. Kyun Kim, F. Bien, C. Young Lee, J.U. Park, Wearable smart sensor systems integrated on soft contact lenses for wireless ocular diagnostics, Nat. Commun. 8 (2017) 14997. https://doi.org/10.1038/ncomms14997.
[14] J. Kim, S. Imani, W.R. de Araujo, J. Warchall, G. Valdes-Ramirez, T.R. Paixao, P.P. Mercier, J. Wang, Wearable salivary uric acid mouthguard biosensor with integrated wireless electronics, Biosens. Bioelectron. 74 (2015) 1061. https://doi.org/10.1016/j.bios.2015.07.039.
[15] A. Mena-Bravo, M.D. Luque de Castro, Sweat: a sample with limited present applications and promising future in metabolomics, J. Pharmaceut. Biomed. Anal. 90 (2014) 139. https://doi.org/10.1016/j.jpba.2013.10.048.
[16] S. Samavat, J. Lloyd, L. O'Dea, W. Zhang, E. Preedy, S. Luzio, K.S. Teng, Uniform sensing layer of immiscible enzyme-mediator compounds developed via a spray aerosol mixing technique towards low cost minimally invasive microneedle continuous glucose monitoring devices, Biosens. Bioelectron. 118 (2018) 224. https://doi.org/10.1016/j.bios.2018.07.054.
[17] E. Larrañeta, R.E.M. Lutton, A.D. Woolfson, R.F. Donnelly, Microneedle arrays as transdermal and intradermal drug delivery systems: materials science, manufacture and commercial development, Mater. Sci. Eng. R Rep. 104 (2016) 1. https://doi.org/10.1016/j.mser.2016.03.001.
[18] T.M. Tuan-Mahmood, M.T. McCrudden, B.M. Torrisi, E. McAlister, M.J. Garland, T.R. Singh, R.F. Donnelly, Microneedles for intradermal and transdermal drug delivery, Eur. J. Pharmaceut. Sci. 50 (2013) 623. https://doi.org/10.1016/j.ejps.2013.05.005.
[19] S. Indermun, R. Luttge, Y.E. Choonara, P. Kumar, L.C. du Toit, G. Modi, V. Pillay, Current advances in the fabrication of microneedles for transdermal delivery, J. Contr. Release 185 (2014) 130. https://doi.org/10.1016/j.jconrel.2014.04.052.
[20] E. Larraneta, M.T. McCrudden, A.J. Courtenay, R.F. Donnelly, Microneedles: a new frontier in nanomedicine delivery, Pharm. Res. 33 (2016) 1055. https://doi.org/10.1007/s11095-016-1885-5.
[21] W. Yuan, H. Xiaoyun, W. Zaozhan, C. Lizhu, Z. Liu, W. Fei, L. Liangming Wei, Dissolving and biodegradable microneedle technologies for transdermal sustained delivery of drug and vaccine, Drug. Des. Devel. Ther. (2013). https://doi.org/10.2147/dddt.S44401.
[22] Y. Luo, Y. Xin, R. Joshi, L. Celi, P. Szolovits, Predicting ICU Mortality Risk by Grouping Temporal Trends from a Multivariate Panel of Physiologic Measurements, AAAI press, Phoenix; United States, 2016, p. 42.
[23] L. Zhao, Z. Wen, F. Jiang, Z. Zheng, S. Lu, Silk/polyols/GOD microneedle based electrochemical biosensor for continuous glucose monitoring, RSC Adv. 10 (2020) 6163. https://doi.org/10.1039/c9ra10374k.
[24] K.B. Kim, W.-C. Lee, C.-H. Cho, D.-S. Park, S.J. Cho, Y.-B. Shim, Continuous glucose monitoring using a microneedle array sensor coupled with a wireless signal transmitter, Sensor. Actuator. B Chem. 281 (2019) 14. https://doi.org/10.1016/j.snb.2018.10.081.
[25] H. Lee, Y.J. Hong, S. Baik, T. Hyeon, D.H. Kim, Enzyme-based glucose sensor: from invasive to wearable device, Adv. Healthc. Mater. 7 (2018), e1701150. https://doi.org/10.1002/adhm.201701150.
[26] S.R. Chinnadayyala, I. Park, S. Cho, Nonenzymatic determination of glucose at near neutral pH values based on the use of nafion and platinum black coated microneedle electrode array, Microchim Acta 185 (2018) 250. https://doi.org/10.1007/s00604-018-2770-1.
[27] Y. Morishita, N. Takama, B. Kim, Fabrication of Porous Biodegradable Microneedles for Glucose Monitoring Sensor, 2018, p. 81.
[28] F. Ribet, G. Stemme, N. Roxhed, Real-time intradermal continuous glucose monitoring using a minimally invasive microneedle-based system, Biomed. Microdevices 20 (2018) 101. https://doi.org/10.1007/s10544-018-0349-6.
[29] H. Lee, T.K. Choi, Y.B. Lee, H.R. Cho, R. Ghaffari, L. Wang, H.J. Choi, T.D. Chung, N. Lu, T. Hyeon, S.H. Choi, D.H. Kim, A graphene-based electrochemical device with thermoresponsive microneedles for diabetes monitoring and therapy, Nat. Nanotechnol. 11 (2016) 566. https://doi.org/10.1038/nnano.2016.38.
[30] K.Y. Hwa, B. Subramani, P.W. Chang, M. Chien, J.T. Huang, Transdermal microneedle array based sensor for real time continous glucose monitoring, Int. J. Electrochem. Sci. 10 (2015).
[31] C. Barrett, K. Dawson, C. O'Mahony, A. O'Riordan, Development of low cost rapid fabrication of sharp polymer microneedles for in vivo glucose biosensing applications, ECS J. Solid State Sci. Technol. 4 (2015) S3053. https://doi.org/10.1149/2.0141510jss.
[32] Y. Yoon, G.S. Lee, K. Yoo, J.B. Lee, Fabrication of a microneedle/CNT hierarchical micro/nano surface electrochemical sensor and its in-vitro glucose sensing characterization, Sensors 13 (2013) 16672. https://doi.org/10.3390/s131216672.
[33] P. Bollella, S. Sharma, A.E.G. Cass, R. Antiochia, Microneedle-based biosensor for minimally-invasive lactate detection, Biosens. Bioelectron. 123 (2019) 152. https://doi.org/10.1016/j.bios.2018.08.010.

[34] A.M.V. Mohan, J.R. Windmiller, R.K. Mishra, J. Wang, Continuous minimally-invasive alcohol monitoring using microneedle sensor arrays, Biosens. Bioelectron. 91 (2017) 574. https://doi.org/10.1016/j.bios.2017.01.016.
[35] C. Hegarty, A. McConville, R.J. McGlynn, D. Mariotti, J. Davis, Design of composite microneedle sensor systems for the measurement of transdermal pH, Mater. Chem. Phys. 227 (2019) 340. https://doi.org/10.1016/j.matchemphys.2019.01.052.
[36] J. Gao, W. Huang, Z. Chen, C. Yi, L. Jiang, Simultaneous detection of glucose, uric acid and cholesterol using flexible microneedle electrode array-based biosensor and multi-channel portable electrochemical analyzer, Sensor. Actuator. B Chem. 287 (2019) 102. https://doi.org/10.1016/j.snb.2019.02.020.
[37] B. Ciui, A. Martin, R.K. Mishra, B. Brunetti, T. Nakagawa, T.J. Dawkins, M. Lyu, C. Cristea, R. Sandulescu, J. Wang, Wearable wireless tyrosinase bandage and microneedle sensors: toward melanoma screening, Adv. Healthc. Mater. 7 (2018), e1701264. https://doi.org/10.1002/adhm.201701264.
[38] P.P. Samant, M.R. Prausnitz, Mechanisms of sampling interstitial fluid from skin using a microneedle patch, Proc. Natl. Acad. Sci. U.S.A. 115 (2018) 4583. https://doi.org/10.1073/pnas.1716772115.
[39] DEXCOM G6 continous glucose monitoring. https://www.dexcom.com/g6-cgm-system. (Accessed 30 June 2020).
[40] Abbott, freestyle Libre 14 day. https://www.freestylelibre.us/system-overview/freestyle-14-day.html#:~:text=The%20FreeStyle%20Libre%2014%20day%20system%20is%20a%20continuous%20glucose,back%20of%20the%20upper%20arm. (Accessed 30 June 2020).
[41] L. Ventrelli, L. Marsilio Strambini, G. Barillaro, Microneedles for transdermal biosensing: current picture and future direction, Adv. Healthc. Mater. 4 (2015) 2606. https://doi.org/10.1002/adhm.201500450.
[42] P.R. Miller, R.J. Narayan, R. Polsky, Microneedle-based sensors for medical diagnosis, J. Mater. Chem. B 4 (2016) 1379. https://doi.org/10.1039/c5tb02421h.
[43] L. Ren, B. Liu, W. Zhou, L. Jiang, A mini review of microneedle array electrode for bio-signal recording: a review, IEEE Sensor. J. 20 (2020) 577. https://doi.org/10.1109/jsen.2019.2944847.
[44] P. Dardano, I. Rea, L. De Stefano, Microneedles-based electrochemical sensors: new tools for advanced biosensing, Curr. Opin. Electrochem. 17 (2019) 121. https://doi.org/10.1016/j.coelec.2019.05.012.
[45] J. Madden, C. O'Mahony, M. Thompson, A. O'Riordan, P. Galvin, Biosensing in dermal interstitial fluid using microneedle based electrochemical devices, Sensing and Bio-Sensing Research (2020). https://doi.org/10.1016/j.sbsr.2020.100348.
[46] F. Jochum, S.J. Moltu, T. Senterre, A. Nomayo, O. Goulet, S. Iacobelli, E.E.E.C.w.g.o.p.p. nutrition, ESPGHAN/ESPEN/ESPR/CSPEN guidelines on pediatric parenteral nutrition: fluid and electrolytes, Clin. Nutr. 37 (2018) 2344. https://doi.org/10.1016/j.clnu.2018.06.948.
[47] M.M. Berger, A. Reintam-Blaser, P.C. Calder, M. Casaer, M.J. Hiesmayr, K. Mayer, J.C. Montejo, C. Pichard, J.-C. Preiser, A.R.H. van Zanten, S.C. Bischoff, P. Singer, Monitoring nutrition in the ICU, Clin. Nutr. 38 (2019) 584. https://doi.org/10.1016/j.clnu.2018.07.009.
[48] E. Scurati-Manzoni, E.F. Fossali, C. Agostoni, E. Riva, G.D. Simonetti, M. Zanolari-Calderari, M.G. Bianchetti, S.A. Lava, Electrolyte abnormalities in cystic fibrosis: systematic review of the literature, Pediatr. Nephrol. 29 (2014) 1015. https://doi.org/10.1007/s00467-013-2712-4.
[49] A. Mishra, R. Greaves, J. Massie, The limitations of sweat electrolyte reference intervals for the diagnosis of cystic fibrosis: a systematic review, Clin. Biochem. Rev. 28 (2007) 60.
[50] M. Odijk, E.J. van der Wouden, W. Olthuis, M.D. Ferrari, E.A. Tolner, A.M.J.M. van den Maagdenberg, A. van den Berg, Microfabricated solid-state ion-selective electrode probe for measuring potassium in the living rodent brain: compatibility with DC-EEG recordings to study spreading depression, Sensor. Actuator. B Chem. 207 (2015) 945. https://doi.org/10.1016/j.snb.2014.06.138.
[51] J.A. Kraut, N.E. Madias, Metabolic acidosis: pathophysiology, diagnosis and management, Nat. Rev. Nephrol. 6 (2010) 274. https://doi.org/10.1038/nrneph.2010.33.
[52] R.M. Forsythe, C.B. Wessel, T.R. Billiar, D.C. Angus, M.R. Rosengart, Parenteral calcium for intensive care unit patients, Cochrane Database Syst. Rev. (2008). https://doi.org/10.1002/14651858.CD006163.pub2.
[53] A. Levin, G.L. Bakris, M. Molitch, M. Smulders, J. Tian, L.A. Williams, D.L. Andress, Prevalence of abnormal serum vitamin D, PTH, calcium, and phosphorus in patients with chronic kidney disease: results of the study to evaluate early kidney disease, Kidney Int. 71 (2007) 31. https://doi.org/10.1038/sj.ki.5002009.
[54] H.Y. Nyein, W. Gao, Z. Shahpar, S. Emaminejad, S. Challa, K. Chen, H.M. Fahad, L.C. Tai, H. Ota, R.W. Davis, A. Javey, A wearable electrochemical platform for noninvasive simultaneous monitoring of Ca^{2+} and pH, ACS Nano 10 (2016) 7216. https://doi.org/10.1021/acsnano.6b04005.
[55] T. Charron, F. Bernard, Y. Skrobik, N. Simoneau, N. Gagnon, M. Leblanc, Intravenous phosphate in the intensive care unit: more aggressive repletion regimens for moderate and severe hypophosphatemia, Intensive Care Med. 29 (2003) 1273. https://doi.org/10.1007/s00134-003-1872-2.
[56] P. Theerawit, Y. Sutherasan, L. Ball, P. Pelosi, Respiratory monitoring in adult intensive care unit, Expet Rev. Respir. Med. 11 (2017) 453. https://doi.org/10.1080/17476348.2017.1325324.
[57] J.S. Krinsley, J.G. Chase, J. Gunst, J. Martensson, M.J. Schultz, F.S. Taccone, J. Wernerman, J. Bohe, C. De Block, T. Desaive, P. Kalfon, J.C. Preiser, Continuous glucose monitoring in the ICU: clinical considerations and consensus, Crit. Care 21 (2017) 197. https://doi.org/10.1186/s13054-017-1784-0.
[58] I.S. Kucherenko, Y.V. Topolnikova, O.O. Soldatkin, Advances in the biosensors for lactate and pyruvate detection for medical applications: a review, Trac. Trends Anal. Chem. 110 (2019) 160. https://doi.org/10.1016/j.trac.2018.11.004.
[59] Z. Song, Y. Xu, Z. Chen, J. Yang, X. Li, Z. Zhang, Quantification of lactate in synovia by microchip with contactless conductivity detection, Anal. Biochem. 434 (2013) 73. https://doi.org/10.1016/j.ab.2012.11.006.
[60] N. Hooman, M. Mehrazma, S. Nakhaii, H. Otukesh, M. Moradi-Lakeh, N. Dianati-Maleki, A. Ehteshami-Afshar, The value of serum uric acid as a mortality prediction in critically ill children, Iran. J. Pediatr. 20 (2010) 323.
[61] A. Fernández-la-Villa, V. Bertrand-Serrador, D.F. Pozo-Ayuso, M. Castaño-Álvarez, Fast and reliable urine analysis using a portable platform based on microfluidic electrophoresis chips with electrochemical detection, Anal. Methods 5 (2013). https://doi.org/10.1039/c2ay26166a.
[62] A.S. Levey, C. Becker, L.A. Inker, Glomerular filtration rate and albuminuria for detection and staging of acute and chronic kidney disease in adults: a systematic review, JAMA 313 (2015) 837. https://doi.org/10.1001/jama.2015.0602.
[63] O. Parlak, S.T. Keene, A. Marais, V.F. Curto, A. Salleo, Molecularly selective nanoporous membrane-based wearable organic electrochemical device for noninvasive cortisol sensing, Sci. Adv. 4 (2018). https://doi.org/10.1126/sciadv.aar2904. eaar2904.
[64] S.K. Arumugasamy, G. Chellasamy, S. Gopi, S. Govindaraju, K. Yun, Current advances in the detection of neurotransmitters by nanomaterials: an update, Trac. Trends Anal. Chem. 123 (2020). https://doi.org/10.1016/j.trac.2019.115766.
[65] R. Zhai, C.C. Sheu, L. Su, M.N. Gong, P. Tejera, F. Chen, Z. Wang, M.P. Convery, B.T. Thompson, D.C. Christiani, Serum bilirubin levels on ICU admission are associated with ARDS development and mortality in sepsis, Thorax 64 (2009) 784. https://doi.org/10.1136/thx.2009.113464.
[66] M. Sgro, D. Campbell, T. Barozzino, V. Shah, Acute neurological findings in a national cohort of neonates with severe neonatal hyperbilirubinemia, J. Perinatol. 31 (2011) 392. https://doi.org/10.1038/jp.2010.137.
[67] Y. Lee, K. Hwang, Skin thickness of Korean adults, Surg. Radiol. Anat. 24 (2002) 183. https://doi.org/10.1007/s00276-002-0034-5.
[68] G.K. Menon, New Insights into skin structure scratching the surface, Adv. Drug Deliv. Rev. 54 (2002). https://doi.org/10.1016/S0169-409X(02)00121-7.
[69] A. El-Laboudi, N.S. Oliver, A. Cass, D. Johnston, Use of microneedle array devices for continuous glucose monitoring: a review, Diabetes Technol. Therapeut. 15 (2013) 101. https://doi.org/10.1089/dia.2012.0188.
[70] P. Xue, L. Zhang, Z. Xu, J. Yan, Z. Gu, Y. Kang, Blood sampling using microneedles as a minimally invasive platform for biomedical diagnostics, Appl. Mater. Today 13 (2018) 144. https://doi.org/10.1016/j.apmt.2018.08.013.
[71] L.K. Smalls, R.R. Wickett, M.O. Visscher, Effect of dermal thickness, tissue composition, and body site on skin biomechanical properties, Skin Res. Technol. 12 (2006) 43.
[72] C.G. Li, C.Y. Lee, K. Lee, H. Jung, An optimized hollow microneedle for minimally invasive blood extraction, Biomed. Microdevices 15 (2013) 17. https://doi.org/10.1007/s10544-012-9683-2.
[73] G.K. Mani, K. Miyakoda, A. Saito, Y. Yasoda, K. Kajiwara, M. Kimura, K. Tsuchiya, Microneedle pH sensor: direct, label-free, real-time detection of cerebrospinal fluid and bladder pH, ACS Appl. Mater. Interfaces 9 (2017) 21651. https://doi.org/10.1021/acsami.7b04225.
[74] S. Bhatnagar, K. Dave, V.V.K. Venuganti, Microneedles in the clinic, J. Contr. Release 260 (2017) 164. https://doi.org/10.1016/j.jconrel.2017.05.029.
[75] T.R.R. Singh, H. McMillan, K. Mooney, A.Z. Alkilani, R.F. Donnelly, Microneedles for drug delivery and monitoring, in: X.J. Li, Y. Zhou (Editors), Microfluidic Devices for Biomedical Applications, 2013, p. 185.
[76] M. Sharma, Transdermal and intravenous nano drug delivery systems, in: S.S. Mohapatra, S. Ranjan, N. Dasgupta, R.K. Mishra, S. Thomas (Editors), Applications of Targeted Nano Drugs and Delivery Systems, 2019, p. 499.
[77] G. Ma, C. Wu, Microneedle, bio-microneedle and bio-inspired microneedle: a review, J. Contr. Release 251 (2017) 11. https://doi.org/10.1016/j.jconrel.2017.02.011.
[78] S.R. Chinnadayyala, K.D. Park, S. Cho, Editors' Choice—review—In vivo and in vitro microneedle based enzymatic and non-enzymatic continuous glucose monitoring biosensors, ECS J. Solid State Sci. Technol. 7 (2018) Q3159. https://doi.org/10.1149/2.0241807jss.
[79] P.R. Miller, R.M. Taylor, B.Q. Tran, G. Boyd, T. Glaros, V.H. Chavez, R. Krishnakumar, A. Sinha, K. Poorey, K.P. Williams, S.S. Branda, J.T. Baca, R. Polsky, Extraction and biomolecular analysis of dermal interstitial fluid collected with hollow microneedles, Commun Biol. 1 (2018) 173. https://doi.org/10.1038/s42003-018-0170-z.
[80] A.E. Cass, S. Sharma, Microneedle enzyme sensor arrays for continuous in vivo monitoring, Methods Enzymol. 589 (2017) 413. https://doi.org/10.1016/bs.mie.2017.02.002.
[81] B.Q. Tran, P.R. Miller, R.M. Taylor, G. Boyd, P.M. Mach, C.N. Rosenzweig, J.T. Baca, R. Polsky, T. Glaros, Proteomic characterization of dermal interstitial fluid extracted using a novel microneedle-assisted technique, J. Proteome Res. 17 (2018) 479. https://doi.org/10.1021/acs.jproteome.7b00642.

[82] M.M. Niedzwiecki, P. Samant, D.I. Walker, V. Tran, D.P. Jones, M.R. Prausnitz, G.W. Miller, Human suction blister fluid composition determined using high-resolution metabolomics, Anal. Chem. 90 (2018) 3786. https://doi.org/10.1021/acs.analchem.7b04073.
[83] C. Chen, X.L. Zhao, Z.H. Li, Z.G. Zhu, S.H. Qian, A.J. Flewitt, Current and emerging technology for continuous glucose monitoring, Sensors 17 (2017). https://doi.org/10.3390/s17010182.
[84] E. Cengiz, W.V. Tamborlane, A tale of two compartments interstitial versus blood glucose monitoring, Diabetes Technol. Therapeut. 11 (2009) 11. https://doi.org/10.1089/dia.2009.0002.
[85] Fogh-Andersen Niels, N.M. Altura, B.T. Altura, O. Siggard-Anderssen, Composition of interstitial fluid, Gen. Clin. Chem. 41 (1995) 1522.
[86] Y. Marunaka, Roles of interstitial fluid pH in diabetes mellitus: glycolysis and mitochondrial function, World J. Diabetes 6 (2015) 125. https://doi.org/10.4239/wjd.v6.i1.125.
[87] A.L. Krogstad, P.A. Jannsson, P. Gisslén, P. Lönnroth, Microdialysis methodology for the measurement of dermal interstitial fluid in humans, Br. J. Dermatol. 134 (1996) 1005.
[88] L. Strindberg, P. Lönnroth, Validation of an endogenous reference technique for the calibration of microdialysis catheters, Scand. J. Clin. Lab. Investig. 60 (2009) 205. https://doi.org/10.1080/003655100750044857.
[89] M.I. Mackness, B. Mackness, S. Arrol, G. Wood, D. Bhatnagar, P.N. Durrington, Presence of paraoxonase in human interstitial fluid, FEBS (Fed. Eur. Biochem. Soc.) Lett. 416 (1997) 377.
[90] W.C. Breckenridge, P. Alaupovic, D.W. Cox, J.A. Little, Apoliprotein and liprotein concentrations in familial, Atherosclerosis 44 (1982) 223. https://doi.org/10.1016/0021-9150(82)90116-2.
[91] D.G. Maggs, R. Jacob, F. Rife, R. Lange, P. Leone, M.J. During, W.V. Tamborlane, R.S. Sherwin, Interstitial fluid concentrations of glycerol, glucose, and amino acids in human quadricep muscle and adipose tissue. Evidence for significant lipolysis in skeletal muscle, J. Clin. Invest. 96 (1995) 370. https://doi.org/10.1172/jci118043.
[92] M.L. Crichton, X. Chen, H. Huang, M.A. Kendall, Elastic modulus and viscoelastic properties of full thickness skin characterised at micro scales, Biomaterials 34 (2013) 2087. https://doi.org/10.1016/j.biomaterials.2012.11.035.
[93] M.A. Kendall, The mechanical properties of the skin epidermis in relation to targeted gene and drug delivery, Biomaterials 28 (2007) 4968. https://doi.org/10.1016/j.biomaterials.2007.08.006.
[94] C. Pailler-Mattei, S. Bec, H. Zahouani, In vivo measurements of the elastic mechanical properties of human skin by indentation tests, Med. Eng. Phys. 30 (2008) 599. https://doi.org/10.1016/j.medengphy.2007.06.011.
[95] B. Chua, S.P. Desai, M.J. Tierney, J.A. Tamada, A.N. Jina, Effect of microneedles shape on skin penetration and minimally invasive continuous glucose monitoring in vivo, Sensor Actuator Phys. 203 (2013) 373. https://doi.org/10.1016/j.sna.2013.09.026.
[96] S.P. Davis, B.J. Landis, Z.H. Adams, M.G. Allen, M.R. Prausnitz, Insertion of microneedles into skin: measurement and prediction of insertion force and needle fracture force, J. Biomech. 37 (2004) 1155. https://doi.org/10.1016/j.jbiomech.2003.12.010.
[97] J.H. Park, M.G. Allen, M.R. Prausnitz, Biodegradable polymer microneedles: fabrication, mechanics and transdermal drug delivery, J. Contr. Release 104 (2005) 51. https://doi.org/10.1016/j.jconrel.2005.02.002.
[98] A.M. Romgens, D.L. Bader, J.A. Bouwstra, F.P.T. Baaijens, C.W.J. Oomens, Monitoring the penetration process of single microneedles with varying tip diameters, J Mech. Behav. Biomed. Mater. 40 (2014) 397. https://doi.org/10.1016/j.jmbbm.2014.09.015.
[99] K.-T. Chang, Y.-K. Shen, F.-Y. Fan, Y. Lin, S.-C. Kang, Optimal design and fabrication of a microneedle arrays patch, J. Manuf. Process. 54 (2020) 274. https://doi.org/10.1016/j.jmapro.2020.02.024.
[100] H.S. Gill, D.D. Denson, B.A. Burris, M.R. Prausnitz, Effect of microneedle design on pain in human volunteers, Clin. J. Pain 24 (2008) 585. https://doi.org/10.1097/AJP.0b013e31816778f9.
[101] D.-S. Lee, C.G. Li, C. Ihm, H. Jung, A three-dimensional and bevel-angled ultrahigh aspect ratio microneedle for minimally invasive and painless blood sampling, Sensor. Actuator. B Chem. 255 (2018) 384. https://doi.org/10.1016/j.snb.2017.08.030.
[102] S. Sharma, Z. Huang, M. Rogers, M. Boutelle, A.E. Cass, Evaluation of a minimally invasive glucose biosensor for continuous tissue monitoring, Anal. Bioanal. Chem. 408 (2016) 8427. https://doi.org/10.1007/s00216-016-9961-6.
[103] J. Trzebinski, S. Sharma, A.R. Moniz, K. Michelakis, Y. Zhang, A.E. Cass, Microfluidic device to investigate factors affecting performance in biosensors designed for transdermal applications, Lab Chip 12 (2012) 348. https://doi.org/10.1039/c1lc20885c.
[104] N. Vasylieva, S. Marinesco, D. Barbier, A. Sabac, Silicon/SU8 multi-electrode micro-needle for in vivo neurochemical monitoring, Biosens. Bioelectron. 72 (2015) 148. https://doi.org/10.1016/j.bios.2015.05.004.
[105] R.K. Mishra, K.Y. Goud, Z. Li, C. Moonla, M.A. Mohamed, F. Tehrani, H. Teymourian, J. Wang, Continuous opioid monitoring along with nerve agents on a wearable microneedle sensor array, J. Am. Chem. Soc. (2020). https://doi.org/10.1021/jacs.0c01883.
[106] K.Y. Goud, C. Moonla, R.K. Mishra, C. Yu, R. Narayan, I. Litvan, J. Wang, Wearable electrochemical microneedle sensor for continuous monitoring of levodopa: toward Parkinson management, ACS Sens. 4 (2019) 2196. https://doi.org/10.1021/acssensors.9b01127.
[107] R.K. Mishra, A.M. Vinu Mohan, F. Soto, R. Chrostowski, J. Wang, A microneedle biosensor for minimally-invasive transdermal detection of nerve agents, Analyst 142 (2017) 918. https://doi.org/10.1039/c6an02625g.
[108] J.R. Windmiller, N. Zhou, M.C. Chuang, G. Valdes-Ramirez, P. Santhosh, P.R. Miller, R. Narayan, J. Wang, Microneedle array-based carbon paste amperometric sensors and biosensors, Analyst 136 (2011) 1846. https://doi.org/10.1039/c1an00012h.
[109] G. Valdés-Ramírez, Y.-C. Li, J. Kim, W. Jia, A.J. Bandodkar, R. Nuñez-Flores, P.R. Miller, S.-Y. Wu, R. Narayan, J.R. Windmiller, R. Polsky, J. Wang, Microneedle-based self-powered glucose sensor, Electrochem. Commun. 47 (2014) 58. https://doi.org/10.1016/j.elecom.2014.07.014.
[110] P. Miller, M. Moorman, R. Manginell, C. Ashlee, I. Brener, D. Wheeler, R. Narayan, R. Polsky, Towards an integrated microneedle total analysis chip for protein detection, Electroanalysis 28 (2016) 1305. https://doi.org/10.1002/elan.201600063.
[111] P.R. Miller, X. Xiao, I. Brener, D.B. Burckel, R. Narayan, R. Polsky, Microneedle-based transdermal sensor for on-chip potentiometric determination of K^+, Adv. Healthc. Mater. 3 (2014) 876. https://doi.org/10.1002/adhm.201300541.
[112] P.R. Miller, S.A. Skoog, T.L. Edwards, D.M. Lopez, D.R. Wheeler, D.C. Arango, X. Xiao, S.M. Brozik, J. Wang, R. Polsky, R.J. Narayan, Multiplexed microneedle-based biosensor array for characterization of metabolic acidosis, Talanta 88 (2012) 739. https://doi.org/10.1016/j.talanta.2011.11.046.
[113] P.R. Miller, S.D. Gittard, T.L. Edwards, D.M. Lopez, X. Xiao, D.R. Wheeler, N.A. Monteiro-Riviere, S.M. Brozik, R. Polsky, R.J. Narayan, Integrated carbon fiber electrodes within hollow polymer microneedles for transdermal electrochemical sensing, Biomicrofluidics 5 (2011) 13415. https://doi.org/10.1063/1.3569945.
[114] J.R. Windmiller, G. Valdés-Ramírez, N. Zhou, M. Zhou, P.R. Miller, C. Jin, S.M. Brozik, R. Polsky, E. Katz, R. Narayan, J. Wang, Bicomponent microneedle array biosensor for minimally-invasive glutamate monitoring, Electroanalysis 23 (2011) 2302. https://doi.org/10.1002/elan.201100361.
[115] P. Bollella, S. Sharma, A.E.G. Cass, F. Tasca, R. Antiochia, Minimally invasive glucose monitoring using a highly porous gold microneedles-based biosensor: characterization and application in artificial interstitial fluid, Catalysts 9 (2019). https://doi.org/10.3390/catal9070580.
[116] P. Bollella, S. Sharma, A.E.G. Cass, R. Antiochia, Minimally-invasive microneedle-based biosensor array for simultaneous lactate and glucose monitoring in artificial interstitial fluid, Electroanalysis 31 (2019) 374. https://doi.org/10.1002/elan.201800630.
[117] S. Sharma, A. Saeed, C. Johnson, N. Gadegaard, A.E.G. Cass, Rapid, low cost prototyping of transdermal devices for personal healthcare monitoring, Sens. Bio-Sensing Res. 13 (2017) 104. https://doi.org/10.1016/j.sbsr.2016.10.004.
[118] T.M. Rawson, S. Sharma, P. Georgiou, A. Holmes, A. Cass, D. O'Hare, Towards a minimally invasive device for beta-lactam monitoring in humans, Electrochem. Commun. 82 (2017) 1. https://doi.org/10.1016/j.elecom.2017.07.011.
[119] S. Song, J. Na, M. Jang, H. Lee, H.-S. Lee, Y.-B. Lim, H. Choi, Y. Chae, A CMOS VEGF sensor for cancer diagnosis using a peptide aptamer-based functionalized microneedle, IEEE Trans. Biomed. Circ. Syst. 13 (2019) 1288. https://doi.org/10.1109/tbcas.2019.2954846.
[120] L. Ren, Q. Jiang, Z. Chen, K. Chen, S. Xu, J. Gao, L. Jiang, Flexible microneedle array electrode using magnetorheological drawing lithography for bio-signal monitoring, Sensor Actuator Phys. 268 (2017) 38. https://doi.org/10.1016/j.sna.2017.10.042.
[121] Z. Chen, L. Ren, J. Li, L. Yao, Y. Chen, B. Liu, L. Jiang, Rapid fabrication of microneedles using magnetorheological drawing lithography, Acta Biomater. 65 (2018) 283. https://doi.org/10.1016/j.actbio.2017.10.030.
[122] E. Skaria, B.A. Patel, M.S. Flint, K.W. Ng, Poly(lactic acid)/carbon nanotube composite microneedle arrays for dermal biosensing, Anal. Chem. 91 (2019) 4436. https://doi.org/10.1021/acs.analchem.8b04980.
[123] D.H. Keum, H.S. Jung, T. Wang, M.H. Shin, Y.E. Kim, K.H. Kim, G.O. Ahn, S.K. Hahn, Microneedle biosensor for real-time electrical detection of nitric oxide for in situ cancer diagnosis during endomicroscopy, Adv Healthc Mater 4 (2015) 1153. https://doi.org/10.1002/adhm.201500012.
[124] Q. Jin, H.J. Chen, X. Li, X. Huang, Q. Wu, G. He, T. Hang, C. Yang, Z. Jiang, E. Li, A. Zhang, Z. Lin, F. Liu, X. Xie, Reduced graphene oxide nanohybrid-assembled microneedles as mini-invasive electrodes for real-time transdermal biosensing, Small 15 (2019), e1804298. https://doi.org/10.1002/smll.201804298.
[125] H. Jia, J. Zhao, L. Qin, M. Zhao, G. Liu, The fabrication of an Ni6MnO8 nanoflake-modified acupuncture needle electrode for highly sensitive ascorbic acid detection, RSC Adv. 9 (2019) 26843. https://doi.org/10.1039/c9ra03850g.
[126] D. Saadat-Moghaddam, J.H. Kim, A microneedle functionalized with polyethyleneimine and nanotubes for highly sensitive, label-free quantification of DNA, Sensors 17 (2017) 1883. https://doi.org/10.3390/s17081883.
[127] Y. Li, H. Zhang, R. Yang, Y. Laffitte, U. Schmill, W. Hu, M. Kaddoura, E.J.M. Blondeel, B. Cui, Fabrication of sharp silicon hollow microneedles by deep-reactive ion etching towards minimally invasive diagnostics, Microsyst. Nanoeng. 5 (2019) 41. https://doi.org/10.1038/s41378-019-0077-y.
[128] M. Senel, M. Dervisevic, N.H. Voelcker, Gold microneedles fabricated by casting of gold ink used for urea sensing, Mater. Lett. 243 (2019) 50. https://doi.org/10.1016/j.matlet.2019.02.014.
[129] F. Liu, Z. Lin, Q. Jin, Q. Wu, C. Yang, H.J. Chen, Z. Cao, D.A. Lin, L. Zhou, T. Hang, G. He, Y. Xu, W. Xia, J. Tao, X. Xie, Protection of nanostructures-integrated

microneedle biosensor using dissolvable polymer coating, ACS Appl. Mater. Interfaces 11 (2019) 4809. https://doi.org/10.1021/acsami.8b18981.
[130] C. Hegarty, S. McKillop, R.J. McGlynn, R.B. Smith, A. Mathur, J. Davis, Microneedle array sensors based on carbon nanoparticle composites: interfacial chemistry and electroanalytical properties, J. Mater. Sci. 54 (2019) 10705. https://doi.org/10.1007/s10853-019-03642-1.
[131] A. Caliò, P. Dardano, V. Di Palma, M.F. Bevilacqua, A. Di Matteo, H. Iuele, L. De Stefano, Polymeric microneedles based enzymatic electrodes for electrochemical biosensing of glucose and lactic acid, Sensor. Actuator. B Chem. 236 (2016) 343. https://doi.org/10.1016/j.snb.2016.05.156.
[132] R.L. Smith, S.D. Collins, J. Duy, T.D. Minogue, Silicon Microneedle Array for Minimally Invasive Human Health Monitoring, SPIE-Int Soc Optical Engineering, San Francisco, CA, 2018.
[133] P. Vazquez, G. Herzog, C. O'Mahony, J. O'Brien, J. Scully, A. Blake, C. O'Mathuna, P. Galvin, Microscopic gel−liquid interfaces supported by hollow microneedle array for voltammetric drug detection, Sensor. Actuator. B Chem. 201 (2014) 572. https://doi.org/10.1016/j.snb.2014.04.080.
[134] K.B. Kim, H. Choi, H.J. Jung, Y.J. Oh, C.H. Cho, J.H. Min, S. Yoon, J. Kim, S.J. Cho, H.J. Cha, Mussel-inspired enzyme immobilization and dual real-time compensation algorithms for durable and accurate continuous glucose monitoring, Biosens. Bioelectron. 143 (2019) 111622. https://doi.org/10.1016/j.bios.2019.111622.
[135] K. Nagamine, J. Kubota, H. Kai, Y. Ono, M. Nishizawa, An array of porous microneedles for transdermal monitoring of intercellular swelling, Biomed. Microdevices 19 (2017) 68. https://doi.org/10.1007/s10544-017-0207-y.
[136] K.B. Mirza, C. Zuliani, B. Hou, F.S. Ng, N.S. Peters, C. Toumazou, Injection Moulded Microneedle Sensor for Real-Time Wireless pH Monitoring, Institute of Electrical and Electronics Engineers Inc, South Korea, 2017, p. 189.
[137] C. Zuliani, F.S. Ng, A. Alenda, A. Eftekhar, N.S. Peters, C. Toumazou, An array of individually addressable micro-needles for mapping pH distributions, Analyst 141 (2016) 4659. https://doi.org/10.1039/c6an00639f.
[138] M. Parrilla, M. Cuartero, S. Padrell Sanchez, M. Rajabi, N. Roxhed, F. Niklaus, G.A. Crespo, Wearable all-solid-state potentiometric microneedle patch for intradermal potassium detection, Anal. Chem. 91 (2019) 1578. https://doi.org/10.1021/acs.analchem.8b04877.
[139] M.A. Invernale, B.C. Tang, R.L. York, L. Le, D.Y. Hou, D.G. Anderson, Microneedle electrodes toward an amperometric glucose-sensing smart patch, Adv. Healthc. Mater. 3 (2014) 338. https://doi.org/10.1002/adhm.201300142.
[140] D. Chen, C. Wang, W. Chen, Y. Chen, J.X. Zhang, PVDF-Nafion nanomembranes coated microneedles for in vivo transcutaneous implantable glucose sensing, Biosens. Bioelectron. 74 (2015) 1047. https://doi.org/10.1016/j.bios.2015.07.036.
[141] S.A. Skoog, P.R. Miller, R.D. Boehm, A.V. Sumant, R. Polsky, R.J. Narayan, Nitrogen-incorporated ultrananocrystalline diamond microneedle arrays for electrochemical biosensing, Diam. Relat. Mater. 54 (2015) 39. https://doi.org/10.1016/j.diamond.2014.11.016.
[142] A. Jina, M.J. Tierney, J.A. Tamada, S. McGill, S. Desai, B. Chua, A. Chang, M. Christiansen, Design, development, and evaluation of a novel microneedle array-based continuous glucose monitor, J. Diabetes Sci. Technol. 8 (2014) 483. https://doi.org/10.1177/1932296814526191.
[143] R. Canovas, S. Padrell Sanchez, M. Parrilla, M. Cuartero, G.A. Crespo, Cytotoxicity study of ionophore-based membranes: toward on-body and in vivo ion sensing, ACS Sens. 4 (2019) 2524. https://doi.org/10.1021/acssensors.9b01322.
[144] L. Tang, Y. Li, H. Xie, Q. Shu, F. Yang, Y.L. Liu, F. Liang, H. Wang, W. Huang, G.J. Zhang, A sensitive acupuncture needle microsensor for real-time monitoring of nitric oxide in acupoints of rats, Sci. Rep. 7 (2017) 6446. https://doi.org/10.1038/s41598-017-06657-3.
[145] M. Wang, L. Hu, C. Xu, Recent advances in the design of polymeric microneedles for transdermal drug delivery and biosensing, Lab Chip 17 (2017) 1373. https://doi.org/10.1039/c7lc00016b.
[146] K.B. Kim, W.-C. Lee, C.-H. Cho, D.-S. Park, S.J. Cho, Y.-B. Shim, Continuous glucose monitoring using a microneedle array sensor coupled with a wireless signal transmitter, Sensor. Actuator. B Chem. 281 (2019) 14. https://doi.org/10.1016/j.snb.2018.10.081.
[147] S. Sharma, A. El-Laboudi, M. Reddy, N. Jugnee, S. Sivasubramaniyam, M. El Sharkawy, P. Georgiou, D. Johnston, N. Oliver, A.E.G. Cass, A pilot study in humans of microneedle sensor arrays for continuous glucose monitoring, Anal. Methods 10 (2018) 2088. https://doi.org/10.1039/c8ay00264a.
[148] S.A.N. Gowers, D.M.E. Freeman, T.M. Rawson, M.L. Rogers, R.C. Wilson, A.H. Holmes, A.E. Cass, D. O'Hare, Development of a minimally invasive microneedle-based sensor for continuous monitoring of beta-lactam antibiotic concentrations in vivo, ACS Sens. 4 (2019) 1072. https://doi.org/10.1021/acssensors.9b00288.
[149] L. Rivas, S. Dulay, S. Miserere, L. Pla, S.B. Marin, J. Parra, E. Eixarch, E. Gratacos, M. Illa, M. Mir, J. Samitier, Micro-needle implantable electrochemical oxygen sensor: ex-vivo and in-vivo studies, Biosens. Bioelectron. 153 (2020) 112028. https://doi.org/10.1016/j.bios.2020.112028.
[150] T. Guinovart, G.A. Crespo, F.X. Rius, F.J. Andrade, A reference electrode based on polyvinyl butyral (PVB) polymer for decentralized chemical measurements, Anal. Chim. Acta 821 (2014) 72. https://doi.org/10.1016/j.aca.2014.02.028.
[151] K.Y. Hwa, B. Subramani, P.W. Chang, M. Chien, J.T. Huang, Transdermal microneedle array based sensor for real time continous glucose monitoring, Int. J. Electrochem. Sci. 10 (2015) 2455.
[152] P. Dardano, A. Caliò, V. Di Palma, M.F. Bevilacqua, A. Di Matteo, L. De Stefano, Multianalyte Biosensor Patch Based on Polymeric Microneedles, Springer Verlag, Rome, Italy, 2018, p. 73.
[153] J.X. Zhou, L.N. Tang, F. Yang, F.X. Liang, H. Wang, Y.T. Li, G.J. Zhang, MoS2/Pt nanocomposite-functionalized microneedle for real-time monitoring of hydrogen peroxide release from living cells, Analyst 142 (2017) 4322. https://doi.org/10.1039/c7an01446e.
[154] A. Moya, X. Guimerà, F.J. del Campo, E. Prats-Alfonso, A.D. Dorado, M. Baeza, R. Villa, D. Gabriel, X. Gamisans, G. Gabriel, Profiling of oxygen in biofilms using individually addressable disk microelectrodes on a microfabricated needle, Microchim. Acta 182 (2015) 985. https://doi.org/10.1007/s00604-014-1405-4.
[155] J.X. Zhou, F. Ding, L.N. Tang, T. Li, Y.H. Li, Y.J. Zhang, H.Y. Gong, Y.T. Li, G.J. Zhang, Monitoring of pH changes in a live rat brain with MoS2/PAN functionalized microneedles, Analyst 143 (2018) 4469. https://doi.org/10.1039/c8an01149d.
[156] M. Sharifian, N. Ashraf, M.H.A. Zavar, M. Chamsaz, F. Afzali, Microneedle copper (II) selective electrode based on polypyrrole doped with 8-hydroxyquinoline-5-sulfonic acid, J. Electrochem. Soc. 162 (2014) B57. https://doi.org/10.1149/2.0371503jes.
[157] T.M. Rawson, S.A.N. Gowers, D.M.E. Freeman, R.C. Wilson, S. Sharma, M. Gilchrist, A. MacGowan, A. Lovering, M. Bayliss, M. Kyriakides, P. Georgiou, A.E.G. Cass, D. O'Hare, A.H. Holmes, Microneedle biosensors for real-time, minimally invasive drug monitoring of phenoxymethylpenicillin: a first-in-human evaluation in healthy volunteers, Lancet Digital Health 1 (2019) e335. https://doi.org/10.1016/s2589-7500(19)30131-1.
[158] R. Esfandyarpour, H. Esfandyarpour, M. Javanmard, J.S. Harris, R.W. Davis, Microneedle biosensor: a method for direct label-free real time protein detection, Sensor. Actuator. B Chem. 177 (2013) 848. https://doi.org/10.1016/j.snb.2012.11.064.
[159] L.C. Clark, C. Lyons, Electrode systems for continuous monitoring in cardiovascular surgery, Ann. N. Y. Acad. Sci. 102 (1962) 29. https://doi.org/10.1111/j.1749-6632.1962.tb13623.x.
[160] T.J. Smith, M.A. Wilson, J.P. Karl, K. Austin, A. Bukhari, S.M. Pasiakos, K.L. O'Connor, H.R. Lieberman, Interstitial glucose concentrations and hypoglycemia during 2 days of caloric deficit and sustained exercise: a double-blind, placebo-controlled trial, J. Appl. Physiol. 121 (2016) 1208. https://doi.org/10.1152/japplphysiol.00432.2016.
[161] J.P. Bantle, W. Thomas, Glucose measurement in patients with diabetes mellitus with dermal interstitial fluid, J. Lab. Clin. Med. 130 (1997) 436. https://doi.org/10.1016/S0022-2143(97)90044-5.
[162] J.I. Reyes-De-Corcuera, H.E. Olstad, R. Garcia-Torres, Stability and stabilization of enzyme biosensors: the key to successful application and commercialization, Annu Rev Food Sci Technol 9 (2018) 293. https://doi.org/10.1146/annurev-food-030216-025713.
[163] M. Parrilla, I. Ortiz-Gomez, R. Canovas, A. Salinas-Castillo, M. Cuartero, G.A. Crespo, Wearable potentiometric ion patch for on-body electrolyte monitoring in sweat: toward a validation strategy to ensure physiological relevance, Anal. Chem. 91 (2019) 8644. https://doi.org/10.1021/acs.analchem.9b02126.
[164] W.E. Huckabee, Control of concentration gradients of pyruvate and lactate across cell membranes in blood, J. Appl. Physiol. 9 (1956) 163. https://doi.org/10.1152/jappl.1956.9.2.163.
[165] E.V. Karpova, A.I. Laptev, E.A. Andreev, E.E. Karyakina, A.A. Karyakin, Relationship between sweat and blood lactate levels during exhaustive physical exercise, ChemElectroChem 7 (2020) 191. https://doi.org/10.1002/celc.201901703.
[166] Y.L. Liu, R. Liu, Y. Qin, Q.F. Qiu, Z. Chen, S.B. Cheng, W.H. Huang, Flexible electrochemical urea sensor based on surface molecularly imprinted nanotubes for detection of human sweat, Anal. Chem. 90 (2018) 13081. https://doi.org/10.1021/acs.analchem.8b04223.
[167] W.S. Waring, A.F.L. Stephen, O.D.G. Robinson, M.A. Dow, J.M. Pettie, Serum urea concentration and the risk of hepatotoxicity after paracetamol overdose, QJM 101 (2008) 359. https://doi.org/10.1093/qjmed/hcn023.
[168] L.M. Ebah, I. Read, A. Sayce, J. Morgan, C. Chaloner, P. Brenchley, S. Mitra, Reverse iontophoresis of urea in health and chronic kidney disease: a potential diagnostic and monitoring tool? Eur. J. Clin. Invest. 42 (2012) 840. https://doi.org/10.1111/j.1365-2362.2012.02657.x.
[169] Nissan drunk-driving prevention concept car. https://www.nissan-global.com/EN/TECHNOLOGY/OVERVIEW/dpcc.html#:~:text=A%20hi%2Dsensitivity%20alcohol%20sensor,she%20attempts%20to%20start%20driving.&text=A%20%22drunk%2Ddriving%22%20voice,via%20the%20car%20navigation%20system. (Accessed 28 July 2020).
[170] R.B. Postuma, D. Berg, M. Stern, W. Poewe, C.W. Olanow, W. Oertel, J. Obeso, K. Marek, I. Litvan, A.E. Lang, G. Halliday, C.G. Goetz, T. Gasser, B. Dubois, P. Chan, B.R. Bloem, C.H. Adler, G. Deuschl, MDS clinical diagnostic criteria for Parkinson's disease, Mov. Disord. 30 (2015) 1591. https://doi.org/10.1002/mds.26424.
[171] Y. Doi, H.F. Chambers, Penicillins and β-lactamase inhibitors, in: J.E. Bennett, R. Dolin, M.J. Blaser (Editors), Basic Principles in the Diagnosis and Management of Infectious Diseases, 2015, p. 4320.
[172] D.W. Hwang, S. Lee, M. Seo, T.D. Chung, Recent advances in electrochemical non-enzymatic glucose sensors - a review, Anal. Chim. Acta 1033 (2018) 1. https://doi.org/10.1016/j.aca.2018.05.051.

[173] B. Halliwell, M.V. Clement, L.H. Long, Hydrogen peroxide in the human body, FEBS (Fed. Eur. Biochem. Soc.) Lett. 486 (2000) 10. https://doi.org/10.1016/S0014-5793(00)02197-9.
[174] J.R. Windmiller, N. Zhou, M.C. Chuang, G. Valdes-Ramirez, P. Santhosh, P.R. Miller, R. Narayan, J. Wang, Microneedle array-based carbon paste amperometric sensors and biosensors, Analyst 136 (2011) 1846. https://doi.org/10.1039/c1an00012h.
[175] E.I. Solomon, D.E. Heppner, E.M. Johnston, J.W. Ginsbach, J. Cirera, M. Qayyum, M.T. Kieber-Emmons, C.H. Kjaergaard, R.G. Hadt, L. Tian, Copper active sites in biology, Chem. Rev. 114 (2014) 3659. https://doi.org/10.1021/cr400327t.
[176] W. Gao, S. Emaminejad, H.Y.Y. Nyein, S. Challa, K. Chen, A. Peck, H.M. Fahad, H. Ota, H. Shiraki, D. Kiriya, D.H. Lien, G.A. Brooks, R.W. Davis, A. Javey, Fully integrated wearable sensor arrays for multiplexed in situ perspiration analysis, Nature 529 (2016) 509. https://doi.org/10.1038/nature16521.
[177] X. Zhang, G. Chen, F. Bian, L. Cai, Y. Zhao, Encoded microneedle arrays for detection of skin interstitial fluid biomarkers, Adv. Mater. 31 (2019). https://doi.org/10.1002/adma.201902825.
[178] E. Caffarel-Salvador, A.J. Brady, E. Eltayib, T. Meng, A. Alonso-Vicente, P. Gonzalez-Vazquez, B.M. Torrisi, E.M. Vicente-Perez, K. Mooney, D.S. Jones, S.E. Bell, C.P. McCoy, H.O. McCarthy, J.C. McElnay, R.F. Donnelly, Hydrogel-forming microneedle arrays allow detection of drugs and glucose in vivo: potential for use in diagnosis and therapeutic drug monitoring, PloS One 10 (2015), e0145644. https://doi.org/10.1371/journal.pone.0145644.
[179] B. Yang, X. Fang, J. Kong, Engineered microneedles for interstitial fluid cell-free DNA capture and sensing using iontophoretic dual-extraction wearable patch, Adv. Funct. Mater. (2020). https://doi.org/10.1002/adfm.202000591.
[180] M.J. McGrath, C.N. Scanaill, Regulations and standards: considerations for sensor technologies, in: M.J. McGrath, C. Ni Scanaill, D. Nafus (Editors), Sensor Technologies: Healthcare, Wellness, and Environmental Applications, Apress, Berkeley, CA, 2013, p. 115.
[181] F.J. Verbaan, S.M. Bal, D.J. van den Berg, J.A. Dijksman, M. van Hecke, H. Verpoorten, A. van den Berg, R. Luttge, J.A. Bouwstra, Improved piercing of microneedle arrays in dermatomed human skin by an impact insertion method, J. Contr. Release 128 (2008) 80. https://doi.org/10.1016/j.jconrel.2008.02.009.
[182] DEXCOM company. https://www.dexcom.com/sv-SE. (Accessed 30 June 2020).
[183] Abbott company. https://www.abbott.com/. (Accessed 30 June 2020).
[184] MEDTRONIC company. https://www.medtronic-diabetes.com/. (Accessed 30 June 2020).
[185] PK Vitality company. https://www.pkvitality.com/. (Accessed 30 June 2020).
[186] PK Vitality K'Watch glucose. https://www.pkvitality.com/ktrack-glucose/. (Accessed 30 June 2020).
[187] PK Vitality K'Watch athlete. https://www.pkvitality.com/ktrack-athlete/. (Accessed 30 June 2020).
[188] American diabetes association. https://www.diabetes.org/. (Accessed 30 June 2020).